Journal of Asian Earth Sciences 35 (2009) 334–353

Contents lists available at ScienceDirect

Journal of Asian Earth Sciences

journal homepage: www.elsevier.com/locate/jaes

# Tectonic evolution of early Paleozoic HP metamorphic rocks in the North Qilian Mountains, NW China: New perspectives

Shuguang Song [a,*], Yaoling Niu [b], Lifei Zhang [a], Chunjing Wei [a], June G. Liou [c], Li Su [d]

[a] MOE Key Laboratory of Orogenic Belts and Crustal Evolution, School of Earth and Space Sciences, Peking University, Beijing 100871, China
[b] Department of Earth Sciences, Durham University, Durham DH1 3LE, UK
[c] Department of Geological and Environmental Sciences, Stanford University, CA94305-2115, USA
[d] Geologic Lab Centre, Chinese University of Geosciences, Beijing 100083, China

ARTICLE INFO

*Article history:*
Received 1 March 2008
Received in revised form 17 November 2008
Accepted 26 November 2008

*Keywords:*
High-pressure belts
Eclogite
Meta-pelite
Cold oceanic subduction
Early Paleozoic era
North Qilian Mountains

ABSTRACT

The North Qilian Mountain range is one of the three oldest orogenic belts preceded with a cold oceanic subduction-zone so far recognized on Earth with a subduction history from 490 Ma to 440 Ma in rock record. This orogenic belt has received much attention over the past decades. A significantly improved understanding of the tectonic evolution of the orogenic belt is now emerging thanks to detailed mineralogical, petrologic, geochemical and geochronological studies as well as field observations carried out over the past few years. In this paper, we offer new perspectives on the tectonic evolution of the North Qilian orogenesis in terms of subduction-zone metamorphism by integrating existing observations and our new data. We provide fairly comprehensive documentation of various observations to support our interpretations, which will also serve as a convenient guide for the field excursion of the 8th International eclogite conference.

In the North Qilian subduction-zone complex (suture zone), two sub-belts of high-pressure (HP) metamorphism have been distinguished in terms of mineral assemblages, i.e., the low-grade blueschist belt and high-grade blueschist–eclogite belt. The low-grade blueschist belt consists of lawsonite–pumpellyite–glaucophane schist, lawsonite–glaucophanite and minor lawsonite-bearing felsic blueschist with a typical mineral assemblage of Lws + Pmp + Gln + Ab + Chl ± Arg. This assemblage constrains the metamorphic conditions of $T = \sim 250–350$ °C and $P = 0.6–1.1$ GPa. Protoliths of the lawsonite-bearing mafic blueschist are similar to present-day N-type MORB. The high-grade blueschist belt occurs as three slices within the island-arc volcanic complex and consists of blueschist- to eclogite-facies metamorphosed greywacke, basite, serpentinite, meta-pelite, chert and marble. Lawsonite and Mg-carpholite occur in eclogites and meta-pelites, respectively. $P–T$ estimation yields peak metamorphic conditions of $P = 2.2–2.6$ GPa and $T = 460–540$ °C for eclogite and carpholite meta-pelite. Geochemical data suggest that protoliths of mafic blueschist and eclogite in both belts have features of present-day MORB or OIB. These observations indicate that the North Qilian HP metamorphic rocks have experienced a history of seafloor subduction in a cold subduction-zone with a geotherm of ~6–7 °C/km in the early Paleozoic before exhumed at the Late Silurian and Devonian in response to continental collision.



## 1. Introduction

The Phanerozoic Eon was thought to have changed significantly in terms of whole Earth's tectonics and thermal state in comparison with the Precambrian time (e.g., Ernst, 1972; McGovern and Schubert, 1989; Condie, 1997; Maruyama and Liou, 2005; Brown, 2007). Blueschist and low-temperature (LT) eclogite, which exclusively represent remnants of ancient oceanic lithosphere subduction, mainly occur in Phanerozoic orogenic belts; only three Precambrian blueschist (without LT eclogite) localities are known (Liou et al., 1990; Maruyama et al., 1996). Furthermore, Paleozoic blueschist and LT eclogite are relatively rare compared to Mesozoic–Cenozoic blueschists possibly due to warmer geothermal gradients at that time and/or subsequent reequilibration (Ernst, 1972; Agard et al., 2005).

The North Qilian Mountain belt is a NW–SE trending Caledonian orogenic belt at the northern margin of the Qinghai-Xizang (Tibetan) Plateau. This orogenic belt has been considered as a material record of a typical oceanic-type subduction-zone in the early Paleozoic (e.g., Xiao et al., 1978; Li et al., 1978; Wu et al., 1993) as it comprises ophiolite suites with zircon SHIRMP U–Pb ages of 495–560 Ma (Yang et al., 2002; Shi et al., 2004; Tseng et al., 2007), calc-alkaline volcanic and I-type granitic rocks (464 ± 8 Ma, Wu et al., 2004), and subduction-zone complexes including HP metamorphic rocks and mélange. Recent studies concur with the earlier notion, but emphasize that

* Corresponding author. Tel.: +86 10 62767729; fax: +86 10 62751159.
*E-mail address:* sgsong@pku.edu.cn (S. Song).

1367-9120/$ - see front matter 
doi:10.1016/j.jseaes.2008.11.005

this belt is an early Paleozoic oceanic suture zone (~440–560 Ma) between the North China Craton (NCC) and the Qilian–Qaidam micro-continent, a fragment of the Rodinia supercontinent (Wan et al., 2001; Song et al., 2006). Wu et al. (1993) reported occurrences of high-grade blueschist with an assemblage of Grt + Gln + Ep + Phn + Ab + Qtz and low-grade blueschist characterized by an assemblage of Gln + Lws + Pmp + Ab + Chl + Arg + Qtz in two distinct areas, and *P–T* estimates of ~340 °C and 0.8 ±0.1 GPa for eclogite lenses within high-grade blueschists (mineral abbreviations after Kretz, 1983). Song (1997) further identified two distinct areas as high-grade blueschist belt and low-grade blueschist belt, respectively. Recent findings of lawsonite-bearing eclogite and carpholite-bearing meta-pelite (Zhang et al., 2007; Song et al., 2007) afford convincing evidence that the North Qilian HP metamorphic belt records cold oceanic lithosphere subduction with a low geothermal gradient (6–7 °C/km) in the early Paleozoic.

In this paper, we present new data on mineral compositions of the low-grade blueschists and marbles, and whole-rock major and trace element compositions of eclogites and blueschists of basaltic protoliths. We use these and existing data in the literature to reevaluate published petrogenetic interpretations of various lithologies in the HP metamorphic belts in North Qilian Mountains. This, together with age data of the ophiolites and HP metamorphism, forms a petrologic framework for an improved understanding of the tectonic evolution of the region in the early Phanerozoic from ocean crust subduction to the continental collision.

## 2. Geological background

The Qilian–Qaidam Mountain region in the northern Qinghai-Tibet Plateau consists of five nearly E-W trending subparallel tectonic units (Fig. 1); from north to south, they are (1) the Alashan block, (2) the North Qilian oceanic-type suture zone, (3) the Qilian block, (4) the North Qaidam *continental-type* UHPM belt, and (5) the Qaidam block. These units were offset by the left-lateral Altyn Tagh Fault system for up to 400 km (Zhang et al., 2001; Yang et al., 2001).

The Alashan block in the western part of the North China Craton consists predominantly of early Precambrian basement with 1.9 Ga granitic gneiss (Xiu et al., 2004) and 1.7–2.7 Ga detrital zircons (Geng et al., 2007; Tung et al., 2007), and is overlain by Cambrian to middle Ordovician cover sequences (Bureau of Geology and Mineral Resources of Ningxia Province, 1990). It was intruded by a ~830 Ma Cu–Ni-bearing ultramafic body (Li et al., 2005). The Qilian block, located between the North Qilian suture zone and the North Qaidam UHPM belt, is an imbricate thrust belt of Precambrian basement overlain by Paleozoic sedimentary sequences. The basement consists of granitic gneiss, marble, amphibolite and minor granulite. Granitic gneisses from the Qilian block have protolith ages of 880–940 Ma (Wan et al., 2001; Xu et al., 2007; Tung et al., 2007), similar to ages of the granitic gneisses in the North Qaidam UHPM Belt. Some Paleoproterozoic granitic gneisses of ~2470 ± 20 Ma have been recognized recently in the Qilian Block (Chen et al., 2007).

The North Qaidam UHPM belt consists of eclogite- and garnet-peridotite-bearing terranes and extends about 400 km along the north Qaidam Mountains. The overall characteristics of rock assemblages, UHP metamorphic evolution and zircon ages suggest that the North Qaidam UHPM belt represents a *continental-type subduction-zone* in the early Paleozoic (see Yang et al., 2002; Song et al., 2003a,b, 2005, 2006; Zhang et al., 2006; Mattinson et al., 2006, 2007).

The Qaidam block to the south is a Mesozoic intra-continental basin with strata deposited on the Precambrian crystalline basement, which may have an affinity with the Yangtze Craton (Zhang et al., 2003).

The North Qilian suture zone is an elongate, NW-trending belt that lies between the Alashan block (north) and the Qilian block (south). As shown in Fig. 2, this suture zone contains early Paleozoic ophiolite sequences, HP metamorphic belts, island-arc volcanic rocks and granitic plutons, Silurian flysch formations, Devonian molasse, and Carboniferous to Triassic sedimentary cover sequences (Wu et al., 1993; Feng and He, 1995; Song, 1996, 1997).

The ophiolite in this suture zone consists of well-preserved sequences of ancient oceanic lithosphere (e.g., Xiao et al., 1978; Feng and He, 1995; Zhang et al., 1997; Qian et al., 2001; Xia et al., 2003; Smith and Yang, 2006; Tseng et al., 2007). Basaltic rocks geochemically resemble present-day N-type and E-type MORB (Feng and He, 1995). Magmatic zircons from cumulated gabbros give U–Pb SHRIMP ages ranging from 496 to 554 Ma (Yang et al., 2002; Shi et al., 2004; Tseng et al., 2007). Two sub-belts of HP metamorphic rocks are readily identified in the suture zone (Wu et al., 1993; Song, 1996): (1) a low-grade blueschist belt with a typical assemblage of Lws + Pmp + Gln + Ab + Chl ± Arg, and (2) a high-grade blueschist belt with an assemblage of Grt + Phn + Gln + Ep that locally encloses massive blocks of eclogite. The protoliths of both blueschist-facies rocks include greywacke, marble, chert and basaltic rocks. SHRIMP U–Pb dating of eclogitic zircons yields ages of 489–464 Ma (Song et al., 2004b, 2006; Zhang et al., 2007), and Ar–Ar ages of glaucophane and phengite from high-grade blueschists range from 462 to 448 Ma (Liou et al., 1989; Wu et al., 1993; Zhang et al., 1997; Liu et al., 2006).

## 3. Low-grade blueschist belt

### 3.1. Occurrence and petrography

The NW-trending low-grade blueschist belt of ~200–500 m wide extends for ~20 km along the Bailong River, ca. 20 km southwest of the town of Sunan (Wu et al., 1990) (see Fig. 2 for locality). It is thrust southwestwards onto the Devonian molasse to the south. To the further south is a large granitic pluton in parallel with the low-grade blueschist belt. To the north of the low-grade blueschist belt is an ophiolitic complex comprised of blocks of serpentinized peridotite, gabbros, pillow lavas and diabasic dykes with thin-layers of radiolarian chert. Copper mineralization is widespread within this ophiolitic complex.

Fig. 3 and Table 1 show the local occurrence and mineral assemblages of low-grade blueschists. Blueschists along the Bailong River are strongly deformed with isoclinal folds and intense foliation on both macro- and micro-scales (Fig. 4a and b). The intensity of deformation decreases gradually northeastwards into non-deformed glaucophane-bearing meta-basalt (Fig. 4c). Protoliths of low-grade blueschists are mainly basaltic rocks with minor felsic ones (Fig. 4d), and no HPM minerals are found in meta-greywackes.

The low-grade blueschists are characterized by HPM assemblages of Lws + Gln + Pmp + Ab (Fig. 4d and e), Lws + Chl + Ab (Fig. 4f), and Pmp + Gln + Chl + Ab. Lawsonite is common in foliated blueschists. Blueschists became less foliated northeastward; some blueschist samples in Tadungou locality retain magmatic clinopyroxene and relic volcanic textures. In Baishuigou Creek (Fig. 3), the massive lawsonite-bearing glaucophanite occurs as a 10 × 20-m-sized block with minor pumpellyite, chlorite and albite (Fig. 4g). Minor aragonite occurs in some blueschist samples. A typical HPM assemblage of Lws + Arg + Ab + Qtz is also found in some metamorphosed pillow basalts (Fig. 4h).

### 3.2. Mineral chemistry

Electron microprobe analyses of minerals were performed on a JEOL JXA-8100 at Peking University, operated at 15 kV acceleration

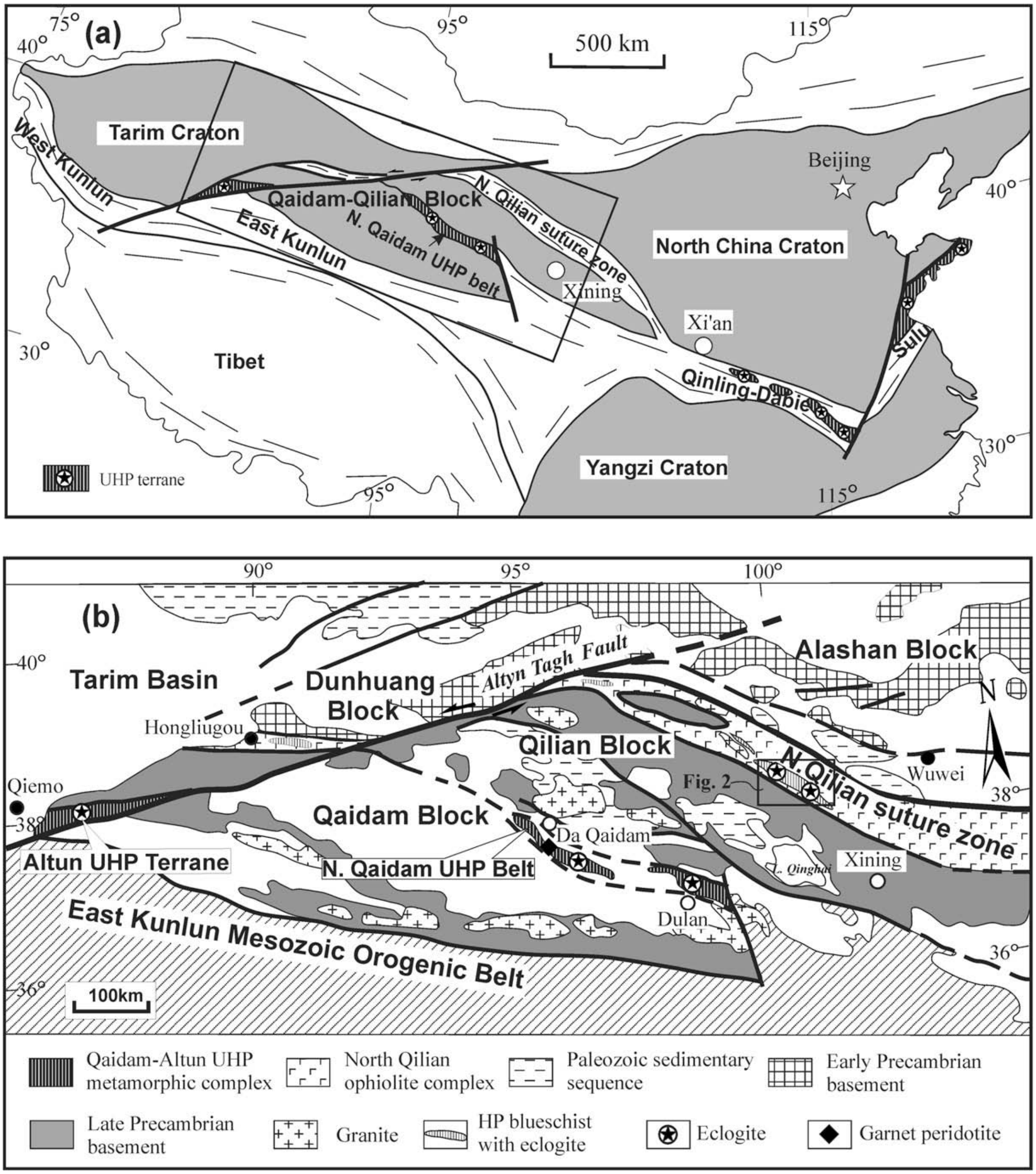


**Fig. 1.** Schematic maps showing major tectonic units of China (a) and subunits of the Qilian–Qaidam orogenic belts in the northern Tibetan Plateau (b) (After Song et al., 2006).

voltage with 20 nA beam current and 1–5 μm beam size. Routine analyses were obtained by counting for 20 s at peak and 5 s on background. Synthetic silica (Si) and spessartine (Mn), natural sanidine (K), pyrope (Mg), andradite (Fe and Ca), albite (Na and Al) and rutile (Ti) were used as calibration standards. Ferric iron in garnet and clinopyroxene was determined based on the scheme of Droop (1987) and $Fe^{3+}$ = Na–(Al + Cr) (Cawthorn and Collerson, 1974), respectively. Normalized pyroxene end-member components were calculated on the basis of jadeite ($X_{Jd}$) = Al/(Na + Ca), aegirine ($X_{Ae}$) = ($Fe^{3+}$)/(Na + Ca) and augite ($X_{Au}$) = (Ca + Mg + $Fe^{2+}$)/2 (Morimoto, 1988). The $Fe^{3+}$ in sodic amphibole was estimated on the basis of structural formulae of 23 oxygen following the charge balance method (Robinson et al., 1982). Total Fe is reported as $Fe^{2+}$ for lawsonite, pumpellyite and white mica. Representative mineral compositions of low-grade blueschists are given in Table 2.

### 3.2.1. Lawsonite

Lawsonite in the low-grade blueschists is euhedral (Fig. 4d–g), and is close to end-member compositions with minor $TiO_2$ (0.05–1.32 wt%), FeO (0.44–0.66 wt%), MnO (0.00–0.05 wt%) and MgO (0.00–0.04 wt%).

### 3.2.2. Glaucophane

Glaucophane of foliated blueschists is fine-grained and occurs in bands differentiated from pumpellyite and lawsonite (Fig. 4b and e). Glaucophane of massive lawsonite-bearing glaucophanite occurs as coarse-grained and zoned euhedral crystals (Fig. 4g) with

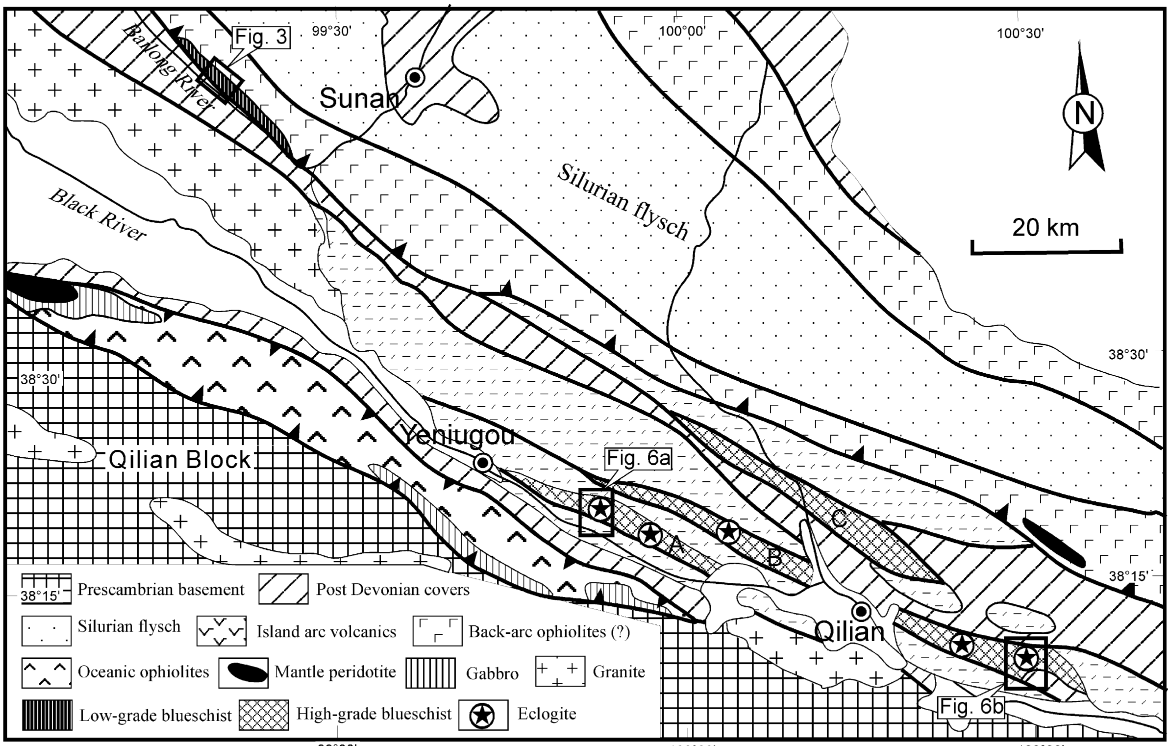


**Fig. 2.** Geological map of the middle part of the North Qilian suture zone.

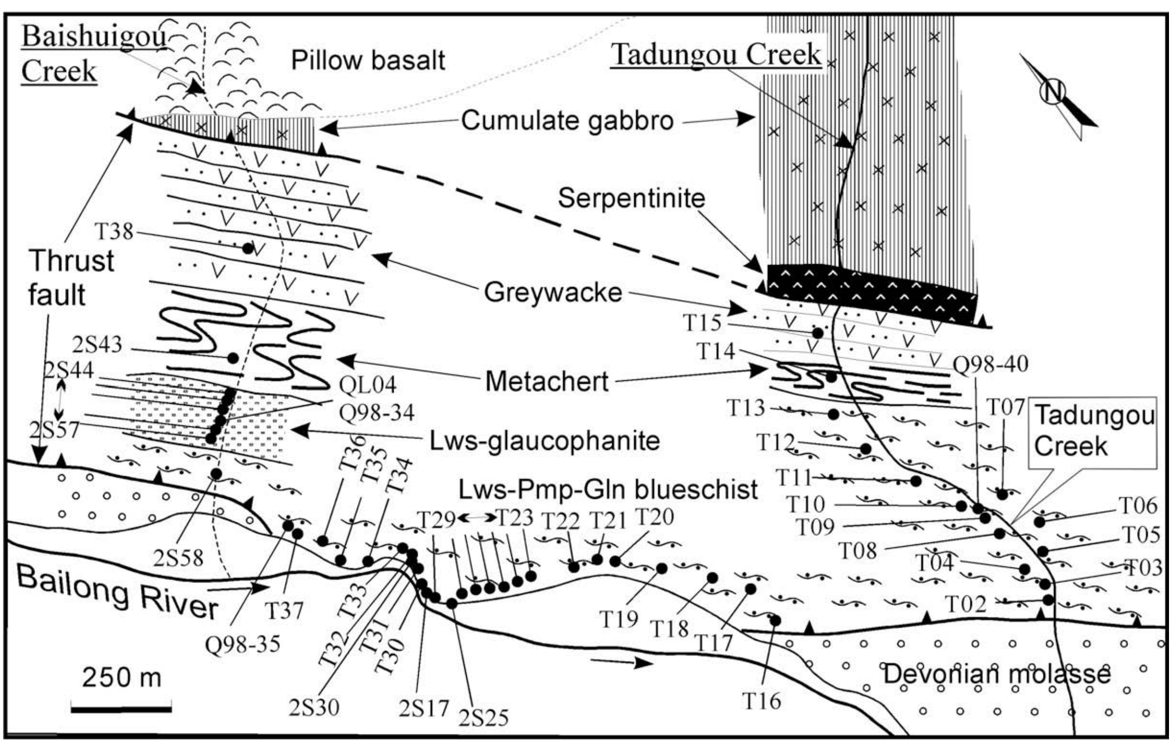


**Fig. 3.** Rock assemblage and sample locations of the low-grade blueschist belt in Bailong River area (see Fig. 2 for its locality).

higher Mg/(Mg + $Fe^{2+}$) ratios towards the rim. In the NaB (Na in the B site) vs. Si and NaB vs. Mg/(Mg + $Fe^{2+}$) diagrams (Fig. 5a), all analyses plot in the glaucophane field with varying Mg/(Mg + $Fe^{2+}$) that is as low as ~0.3.

*3.2.3. Pumpellyite*

Pumpellyite is a ubiquitous phase in equilibrium with glaucophane and lawsonite in the low-grade blueschists. Most pumpellyite crystals are fine-grained (<50 μm) and occur as bands in strongly

**Table 1**
Mineral assemblages of metabasic rocks from the Bailong River area (for sample locality, see Fig. 3).

| Sample | Rock type | Mineral assemblage |
|---|---|---|
| T02 | Blueschist, foliated | Gln, Pmp, Lws, Arg, Chl, Ab |
| T03 | Blueschist, foliated | Gln, Pmp, Chl, Ab |
| T04 | Blueschist, weak foliated | Gln, Pmp, Chl with relic igneous Cpx and Pl |
| T05 | Meta-sedimentary | Chl, Ms (Phn?), Ab, Qtz |
| T06 | Blueschist, weak foliated | Gln, Pmp, Arg, Chl, Stl, Ab with relic igneous Cpx |
| T07 | Meta-basalt, weak foliated | Pmp, Chl with relic igneous Cpx and Pl |
| T08 | Meta-basalt, weak foliated | Gln, Pmp, Chl, Ab with relic igneous Cpx |
| T09 | Meta-basalt, weak foliated | Gln, Pmp, Chl, Ab with relic igneous Cpx |
| Q98-40 | Meta-basalt, weak foliated | Gln, Pmp, Chl, Ab with relic igneous Cpx |
| T10–T12 | Blueschist, foliated | Gln, Pmp, Chl, Stl, Ab |
| T13 | Meta-basalt, weak foliated | Gln, Pmp, Chl, Ms, Ab, Qtz with relic igneous Pl |
| T14 | Meta-chert | Ms, Qtz |
| T15 | Meta-greywacke | Chl, Ep, Ms, Ab, Qtz |
| T16–T22 | Blueschist, foliated | Gln, Pmp, Chl, Ab |
| T23 | Blueschist, foliated | Gln, Lws, Pmp, Arg, Chl, Ab |
| T24 | Blueschist, foliated | Gln, Pmp, Chl, Ab |
| T25 | Blueschist, foliated | Gln, Lws, Pmp, Chl, Ab |
| T26–T28 | Blueschist, foliated | Gln, Pmp, Chl, Ab |
| 2S25 | Blueschist, foliated | Gln, Lws, Pmp, Arg, Ab |
| T29 | Blueschist, foliated | Gln, Lws, Pmp, Arg, Ab |
| 2S17 | Blueschist, foliated | Gln, Lws, Pmp, Arg, Ab |
| T30 | Blueschist, foliated | Gln, Lws, Pmp, Chl, Ab, Qtz |
| T31 | Blueschist, foliated | Gln, Lws, Pmp, Arg, Chl, Ab |
| 2S30 | Blueschist, foliated | Gln, Lws, Pmp, Arg, Chl, Ab |
| T32–T34 | Blueschist, foliated | Gln, Pmp, Chl, Ab |
| T35 | Blueschist, foliated | Gln, Lws, Pmp, Chl, Ab |
| T36 | Blueschist, foliated | Gln, Pmp, Chl, Ab |
| T37 | Blueschist, foliated | Gln, Lws, Pmp, Chl, Ab |
| Q98-35 | Blueschist, foliated | Gln, Lws, Pmp, Chl, Ab |
| 2S38–2S39 | Meta-greywacke | Chl, Ep, Ms, Ab, Qtz |
| 2S43 | Meta-chert | Ms, Qtz |
| 2S44–2S57 | Lws-glaucophanite | Gln, Lws, Pmp, Chl, Ab, Spn |
| QL04 | Lws-glaucophanite | Gln, Lws, Pmp, Chl, Ab, Spn |
| Q98-34 | Lws-glaucophanite | Gln, Lws, Pmp, Chl, Ab, Spn |
| 2S58 | Mylonite | Chl, Ab, Qtz |

deformed samples (Fig. 4b and e). Pumpellyite crystals in the lawsonite glaucophanite are rich in total FeO (9.6–11.6 wt%), whereas those in the foliated blueschist are high in MgO (1.8–3.2 wt%) and relatively low in FeO (3.3–5.5 wt%). Fig. 5b shows the compositional variation of pumpellyite of low-grade blueschists.

*3.2.4. Chlorite*

Chlorite occurs as fine grains between lawsonite and pumpellyite crystals and has mostly pycnochlorite compositions (Wu et al., 1993; this study in Table 2).

*3.2.5. Albite*

Albite is widespread in low-grade blueschist samples. Chemical analyses reveal near pure albite compositions with Ab 97.8–99.5 mol%, An 0–1.9 mol% and Or 0.3–0.5 mol% (Table 2).

*3.3. P–T estimates*

Wu et al. (1993) reported pressure estimates of ~0.6–0.7 GPa for lawsonite-bearing blueschist using diagrams of $Na^{M4}$ versus $A1^{IV}$ in glaucophane (Brown, 1977) and of $Al_2O_3$ (wt%) in glaucophane versus $X_{Fe}$ in chlorite (Maruyama et al., 1986). The first appearance of lawsonite in the presence of excess quartz and $H_2O$ occurs at about 170–180 °C and $P_{H_2O} = P_{Total}$ = 0.4–0.5 GPa (Liou, 1971). Maruyama and Liou (1987) suggested that the stable coexistence of Arg + Lws + Qtz without heulandite could occur at about 150 °C and 0.4 GPa, and Lws + Pmp + Gln at about 200–250 °C and 0.7 GPa. The presence of albite and aragonite in low-grade blueschists constrained the pressures in a range between two reaction curves of Jd + Qtz = Ab and Arg = Cc (Fig. 5c). Pumpellyite, the index mineral for the pumpellyite–prehnite facies metamorphism, first appears at $T$ = ~250 °C by the reaction Lm + Prh + Chl = Pmp + Qtz + $H_2O$ and disappears at $T$ = ~350 °C by the reaction Pmp = Zo + Grs + Chl + $H_2O$ (Schiffman and Liou, 1980; Liou et al., 1987; Fig. 5c). Dehydration of lawsonite at low-pressure ($P$ = ~0.6–1.1 GPa) occurs at temperature ~350–400 °C through a reaction Lws + Ab = Zo + Pa + Qtz + $H_2O$. Therefore, $P–T$ conditions for low-grade blueschist assemblages of Lws + Ab + Qtz + Arg and Lws + Gln + Pmp + Chl ± Arg are best constrained at ~250–350 °C and 0.6–1.1 GPa. Recent $P–T$ pseudosection calculation shows that the metamorphic $P–T$ conditions for low-grade blueschist are limited in the range of 320–375 °C and 0.75–0.95 GPa (Zhang et al., this issue). The variation of mineral assemblages may suggest pressure decrease from southwest to northeast.

## 4. High-grade blueschist belt

As shown in Fig. 2, the high-grade blueschist belt of about 140 km long occurs tectonically as three NW-trending slices A, B and C within arc-type siliceous volcanic rocks (dominantly rhyolite, dacite, andesite and minor basalt). These slices are composed of typical subduction-zone mélange with various blueschist- to eclogite-facies metamorphosed blocks and lenses of limestone and ophiolitic fragments including serpentinite, basalt, pelite and pelagic chert within a blueschist-facies meta-greywacke matrix. Fig. 6 and Table 3 show the locations, rock types and mineral assemblages of the high-grade blueschist belt in two representative cross-sections in Qingshuigou and Baijingsi.

*4.1. Occurrence and petrography*

*4.1.1. Meta-greywackes and olistostrome*

The meta-greywacke matrix of the mélange is typical of an accretionary wedge rock assemblage and constitutes the major

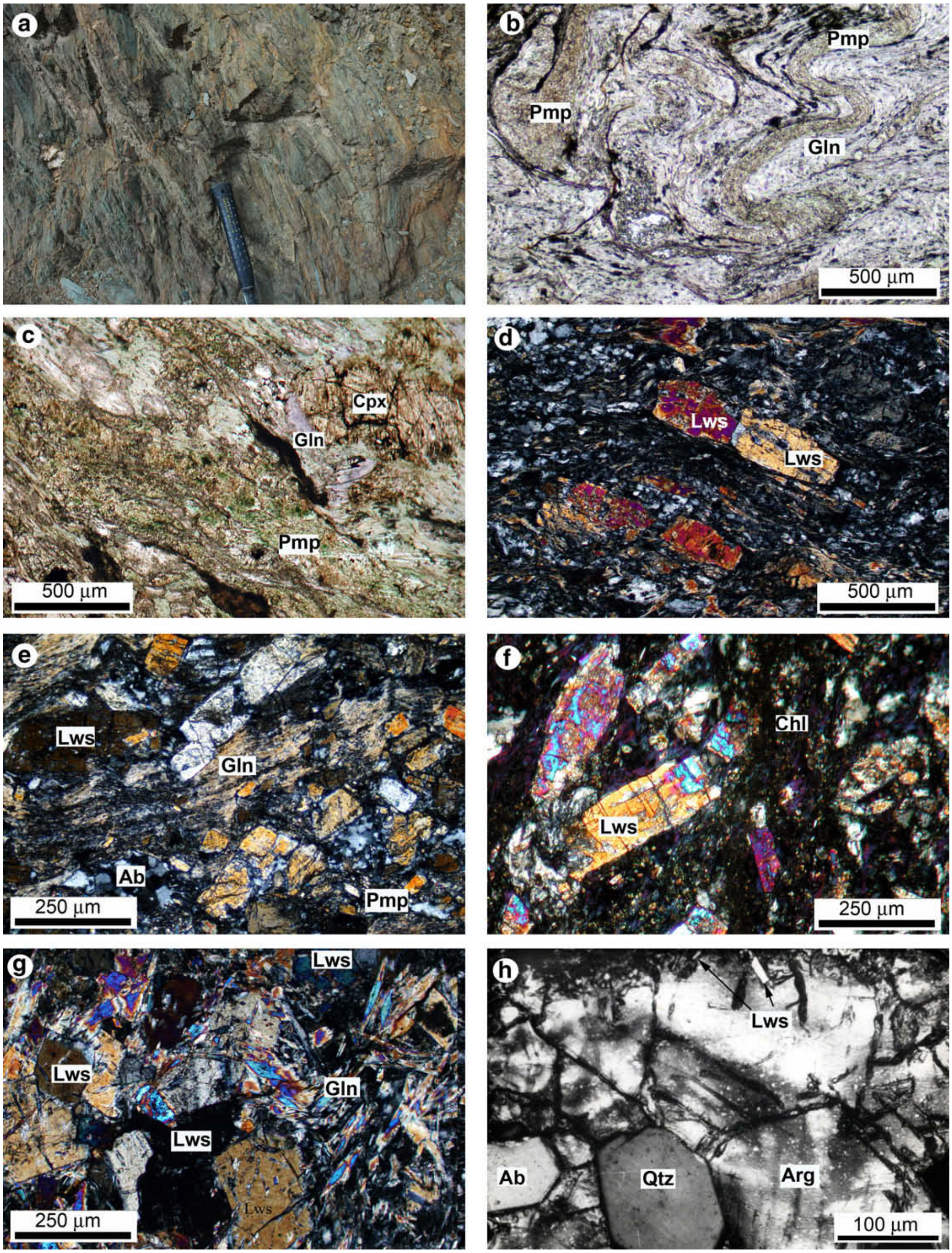


**Fig. 4.** Photographs of low-grade blueschists. (a) Low-grade blueschist outcrop showing isoclinal folds. (b) Micro-folds of glaucophane (Gln) and pumpellyite (Pmp) segregation bands. (c) Pmp + Gln overprinting the primitive Cpx. (d) Lws + Gln in the felsic blueschist; (e) Lws + Gln + Pmp + Ab (+Chl) assemblage with intensive schistosity. (f) Lws + Chl (+Ab) assemblage. (g) Lws + Gln (+Pmp + Chl + Ab) assemblage without schistosity. (h) Lws + Arg + Ab + Qtz assemblage in a metamorphosed pillow basalt sample. Aragonite was confirmed by Raman spectra in Xi'an Institute of Geology and Mineral Resources.

components of the high-grade blueschist belt (Wu et al., 1993; Song, 1997). Meta-greywackes are foliated, and contain a blueschist-facies mineral assemblage of Gln + Phn + Pg + Ep + Ab + Qtz ± Grt. A ~100-m-thick layer of conglomerate with miscellaneous gravels occurs in the south border of Slice A in Qingshuigou cross-section (Fig. 6a) and extends for about 5–8 km. Song (1996) interpreted it as an "olistostrome" deposit. The olistoliths contain variously sized, strongly deformed blocks of marble, meta-chert, serpentinites, and mafic and siliceous volcanic rocks within a greywacke matrix (Fig. 7a).

Blueschist- to eclogite-facies metamorphosed turbidites are also recognized in the high-grade blueschist belt (Fig. 7b and c), and show deformed, interbedded structures with thicker, light-colored layers of meta-sandstone and thinner, dark-colored layers of meta-pelite (blueschist). The meta-sandstone has a mineral assemblage of Grt + Phn + Qtz ± Gln ± Ep.

**Table 2**
Mineral compositions of blueschists in the low-grade blueschist belt.

| Sample | 2S30-1 | 2S30-2 | 2S30-3 | 2S46-1 | 2S46-2 | 2S46-3 | 2S57-1 | QL04-1 | QL04-2 | QL04-3 | 2S30-1 | 2S30-2 | 2S17-1 | 2S17-2 | 2S25 | 2S46 | QL04-1 |
|---|---|---|---|---|---|---|---|---|---|---|---|---|---|---|---|---|---|
| Mineral | Lws | Lws | Lws | Lws | Lws | Lws | Lws | Lws | Lws | Lws | Pmp | Pmp | Pmp | Pmp | Pmp | Pmp | Pmp |
| $SiO_2$ | 38.53 | 38.56 | 38.60 | 39.94 | 40.25 | 39.69 | 39.42 | 38.80 | 38.42 | 38.90 | 36.91 | 37.34 | 37.82 | 37.65 | 36.91 | 37.07 | 36.59 |
| $TiO_2$ | 0.13 | 0.48 | 0.04 | 0.43 | 1.23 | 0.00 | 0.63 | 0.62 | 1.32 | 0.05 | 0.07 | 0.06 | 0.14 | 0.10 | 0.04 | 0.13 | 0.01 |
| $Al_2O_3$ | 31.10 | 31.07 | 31.18 | 31.96 | 31.46 | 31.69 | 32.28 | 30.97 | 30.43 | 31.47 | 24.93 | 23.48 | 25.95 | 25.57 | 24.96 | 25.46 | 22.97 |
| $Cr_2O_3$ | 0.03 | 0.07 | 0.05 | 0.07 | 0.00 | 0.08 | 0.01 | 0.02 | 0.00 | 0.04 | 0.02 | 0.06 | 0.01 | 0.08 | 0.00 | 0.10 | 0.01 |
| FeO | 0.44 | 0.56 | 0.51 | 0.51 | 0.48 | 0.53 | 0.50 | 0.44 | 0.66 | 0.46 | 3.31 | 4.27 | 5.15 | 5.62 | 5.55 | 9.61 | 11.65 |
| MnO | 0.05 | 0.02 | 0.00 | 0.00 | 0.00 | 0.05 | 0.03 | 0.03 | 0.00 | 0.05 | 0.69 | 0.47 | 0.24 | 0.17 | 0.31 | 1.01 | 0.15 |
| MgO | 0.01 | 0.00 | 0.00 | 0.04 | 0.02 | 0.04 | 0.00 | 0.02 | 0.01 | 0.00 | 3.20 | 2.93 | 1.83 | 1.86 | 2.39 | 0.01 | 0.01 |
| CaO | 16.54 | 16.60 | 16.41 | 16.65 | 16.37 | 16.39 | 16.61 | 16.86 | 16.41 | 16.49 | 21.68 | 21.52 | 22.54 | 22.34 | 22.29 | 21.59 | 22.74 |
| $Na_2O$ | 0.08 | 0.04 | 0.15 | 0.00 | 0.00 | 0.02 | 0.01 | 0.06 | 0.04 | 0.03 | 0.21 | 0.23 | 0.10 | 0.09 | 0.05 | 0.00 | 0.07 |
| $K_2O$ | 0.01 | 0.04 | 0.04 | 0.00 | 0.00 | 0.02 | 0.00 | 0.01 | 0.01 | 0.00 | 0.01 | 0.00 | 0.00 | 0.00 | 0.00 | 0.00 | 0.01 |
| Total | 86.92 | 87.43 | 87.01 | 89.60 | 89.82 | 88.52 | 89.55 | 87.87 | 87.33 | 87.53 | 91.09 | 90.36 | 93.79 | 93.48 | 92.50 | 95.01 | 94.31 |
| O | 8 | 8 | 8 | 8 | 8 | 8 | 8 | 8 | 8 | 8 | 12 | 12 | 12 | 12 | 12 | 12 | 12 |
| Si | 2.048 | 2.040 | 2.050 | 2.056 | 2.065 | 2.067 | 2.032 | 2.044 | 2.038 | 2.051 | 2.960 | 3.028 | 2.962 | 2.965 | 2.945 | 2.936 | 2.963 |
| Ti | 0.005 | 0.019 | 0.002 | 0.017 | 0.048 | 0.000 | 0.025 | 0.025 | 0.053 | 0.002 | 0.004 | 0.004 | 0.008 | 0.006 | 0.003 | 0.008 | 0.001 |
| $Al^{IV}$ | 0.000 | 0.000 | 0.000 | 0.000 | 0.000 | 0.000 | 0.000 | 0.000 | 0.000 | 0.000 | 0.040 | 0.000 | 0.038 | 0.035 | 0.055 | 0.064 | 0.037 |
| AlVI | 1.948 | 1.938 | 1.951 | 1.939 | 1.902 | 1.945 | 1.961 | 1.922 | 1.902 | 1.956 | 2.316 | 2.244 | 2.357 | 2.338 | 2.292 | 2.312 | 2.154 |
| Cr | 0.001 | 0.003 | 0.002 | 0.003 | 0.000 | 0.003 | 0.000 | 0.001 | 0.000 | 0.002 | 0.001 | 0.004 | 0.001 | 0.005 | 0.000 | 0.006 | 0.001 |
| $Fe^{2+}$ | 0.020 | 0.025 | 0.023 | 0.022 | 0.021 | 0.023 | 0.022 | 0.019 | 0.029 | 0.020 | 0.222 | 0.290 | 0.337 | 0.370 | 0.370 | 0.636 | 0.789 |
| Mn | 0.002 | 0.001 | 0.000 | 0.000 | 0.000 | 0.002 | 0.001 | 0.001 | 0.000 | 0.002 | 0.047 | 0.032 | 0.016 | 0.011 | 0.021 | 0.068 | 0.010 |
| Mg | 0.001 | 0.000 | 0.000 | 0.003 | 0.002 | 0.003 | 0.000 | 0.002 | 0.001 | 0.000 | 0.383 | 0.354 | 0.214 | 0.218 | 0.284 | 0.001 | 0.001 |
| Ca | 0.942 | 0.941 | 0.934 | 0.918 | 0.900 | 0.914 | 0.917 | 0.951 | 0.933 | 0.932 | 1.863 | 1.870 | 1.891 | 1.885 | 1.905 | 1.832 | 1.972 |
| Na | 0.008 | 0.004 | 0.015 | 0.000 | 0.000 | 0.002 | 0.001 | 0.006 | 0.004 | 0.003 | 0.033 | 0.036 | 0.015 | 0.014 | 0.008 | 0.000 | 0.011 |
| K | 0.001 | 0.003 | 0.003 | 0.000 | 0.000 | 0.001 | 0.000 | 0.001 | 0.001 | 0.000 | 0.001 | 0.000 | 0.000 | 0.000 | 0.000 | 0.000 | 0.001 |
| Sum | 4.976 | 4.974 | 4.981 | 4.957 | 4.937 | 4.961 | 4.963 | 4.974 | 4.961 | 4.970 | 7.874 | 7.862 | 7.840 | 7.847 | 7.883 | 7.865 | 7.947 |

| Sample | 2S46-1 | 2S46-2 | 2S57-1 | 2S57-2 | QL04-1 | QL04-2 | 2S46-1 | 2S46-2 | QL04-1 | 2S46-1 | 2S46-2 | 2S57 |
|---|---|---|---|---|---|---|---|---|---|---|---|---|
| Mineral | Gln (C) | Gln(R) | Gln | Gln | Gln | Gln | Chl | Chl | chl | Ab | Ab | Ab |
| $SiO_2$ | 54.79 | 55.91 | 57.47 | 56.10 | 56.50 | 56.19 | 27.93 | 27.07 | 27.54 | 68.98 | 68.32 | 68.32 |
| $TiO_2$ | 0.00 | 0.10 | 0.09 | 0.22 | 0.11 | 0.19 | 0.00 | 0.00 | 0.00 | 0.08 | 0.00 | 0.00 |
| $Al_2O_3$ | 4.67 | 11.29 | 10.90 | 10.92 | 11.19 | 9.81 | 18.00 | 19.09 | 18.83 | 19.61 | 19.44 | 19.66 |
| FeO | 23.94 | 17.14 | 13.83 | 11.59 | 12.32 | 13.51 | 0.30 | 0.33 | 0.07 | 0.00 | 0.02 | 0.03 |
| $Cr_2O_3$ | 0.22 | 0.21 | 0.02 | 0.00 | 0.03 | 0.06 | 26.73 | 27.08 | 18.54 | 0.17 | 0.16 | 0.07 |
| MnO | 0.32 | 0.43 | 0.13 | 0.10 | 0.12 | 0.15 | 1.09 | 1.17 | 0.49 | 0.02 | 0.02 | 0.00 |
| MgO | 5.59 | 5.40 | 8.63 | 9.13 | 8.87 | 9.00 | 13.12 | 12.67 | 20.77 | 0.00 | 0.02 | 0.00 |
| CaO | 0.82 | 0.95 | 0.94 | 0.96 | 0.57 | 1.09 | 0.14 | 0.10 | 0.08 | 0.27 | 0.39 | 0.00 |
| $Na_2O$ | 7.79 | 7.74 | 6.97 | 7.42 | 7.96 | 6.83 | 0.07 | 0.00 | 0.04 | 11.07 | 10.81 | 11.73 |
| $K_2O$ | 0.02 | 0.03 | 0.00 | 0.02 | 0.02 | 0.01 | 0.02 | 0.00 | 0.01 | 0.06 | 0.05 | 0.09 |
| Total | 98.16 | 99.20 | 98.98 | 96.46 | 97.69 | 96.84 | 87.44 | 87.59 | 86.47 | 100.25 | 99.23 | 99.89 |
| O | 23 | 23 | 23 | 23 | 23 | 23 | 14 | 14 | 14 | 8 | 8 | 8 |
| Si | 7.995 | 7.884 | 7.870 | 7.883 | 7.863 | 7.874 | 2.982 | 2.894 | 2.844 | 3.000 | 3.001 | 2.988 |
| Ti | 0.000 | 0.011 | 0.009 | 0.023 | 0.012 | 0.020 | 0.000 | 0.000 | 0.000 | 0.003 | 0.000 | 0.000 |
| $Al^{IV}$ | 0.005 | 0.116 | 0.130 | 0.117 | 0.137 | 0.126 | 1.018 | 1.106 | 1.156 | 0.000 | 0.000 | 0.012 |
| $Al^{VI}$ | 0.798 | 1.758 | 1.628 | 1.690 | 1.697 | 1.492 | 1.246 | 1.298 | 1.136 | 1.005 | 1.006 | 1.002 |
| Cr | 0.025 | 0.023 | 0.002 | 0.000 | 0.003 | 0.007 | 0.025 | 0.028 | 0.006 | 0.000 | 0.001 | 0.001 |
| $Fe^{3+}$ | 0.718 | 0.000 | 0.355 | 0.066 | 0.092 | 0.403 | 0.000 | 0.000 | 1.601 | 0.000 | 0.000 | 0.000 |
| $Fe^{2+}$ | 2.204 | 2.021 | 1.229 | 1.296 | 1.342 | 1.181 | 2.386 | 2.420 | 0.043 | 0.006 | 0.006 | 0.002 |
| Mn | 0.040 | 0.051 | 0.015 | 0.012 | 0.014 | 0.018 | 0.098 | 0.106 | 0.009 | 0.001 | 0.001 | 0.000 |
| Mg | 1.216 | 1.135 | 1.762 | 1.913 | 1.840 | 1.880 | 2.088 | 2.019 | 3.198 | 0.000 | 0.001 | 0.000 |
| Ca | 0.128 | 0.144 | 0.138 | 0.145 | 0.085 | 0.164 | 0.015 | 0.011 | 0.009 | 0.013 | 0.018 | 0.000 |
| Na | 2.204 | 2.116 | 1.851 | 2.021 | 2.148 | 1.855 | 0.015 | 0.000 | 0.008 | 0.933 | 0.921 | 0.995 |
| K | 0.004 | 0.005 | 0.000 | 0.004 | 0.004 | 0.002 | 0.003 | 0.000 | 0.001 | 0.003 | 0.003 | 0.005 |
| Sum | 15.336 | 15.265 | 14.989 | 15.170 | 15.237 | 15.021 | 9.882 | 9.890 | 10.011 | 4.963 | 4.957 | 5.005 |

C, core; R, rim.

### 4.1.2. Eclogite and mafic blueschist

All mafic blueschists and eclogites occur as blocks or lenses of varying size within felsic blueschists (Fig. 7d). The eclogite blocks are mainly found in slices A and B of the high-grade blueschist belt (Fig. 1). In terms of mineral assemblages, these eclogites can be grouped into two types (Song et al., 2007): (1) phengite-rich eclogite with a peak-stage Grt + Omp + Phn + Rt assemblage plus minor epidote (Fig. 8a), and (2) epidote-rich eclogite with a Grt + Omp + Ep/Cz + Gln + Rt ± Qtz assemblage and minor phengite and paragonite. Most epidote eclogites are strongly deformed, and show elongated epidote/clinozoisite, omphacite and phengitic mica oriented along the foliation overprinting the undeformed assemblage (Fig. 8b). Most eclogite blocks have undergone retrograde blueschist-facies overprinting; some are completely retrograded into mafic blueschist (Grt–Ep–Phn–Gln–Ab schist).

Inclusions of lawsonite and lawsonite pseudomorphs are identified in some porphyroblastic garnets from both eclogite types (Zhang et al., 2007; Song et al., 2007). Lawsonite pseudomorphs show rectangular and triangular shapes and consist of aggregates of Cz + Pg ± Phn ± Omp defining a possible reaction such as Lws + Jd (Omp) = Cz + Pg + $H_2O$ (Fig. 8c). The numerous lawsonite pseudomorphs together with omphacite inclusions in garnet suggest that lawsonite was ubiquitous during the peak stage of eclogite-facies metamorphism associated with "cold" oceanic subduction. *P–T* calculations using the Grt–Omp–Phn(–Ky) geothermobarometry of Ravna and Terry (2004) give a temperature range of 460–510 °C and a pressure range of 2.20–2.60 GPa, which lie mainly in the lawsonite-eclogite field (Song et al., 2004b, 2007; Zhang et al., 2007).

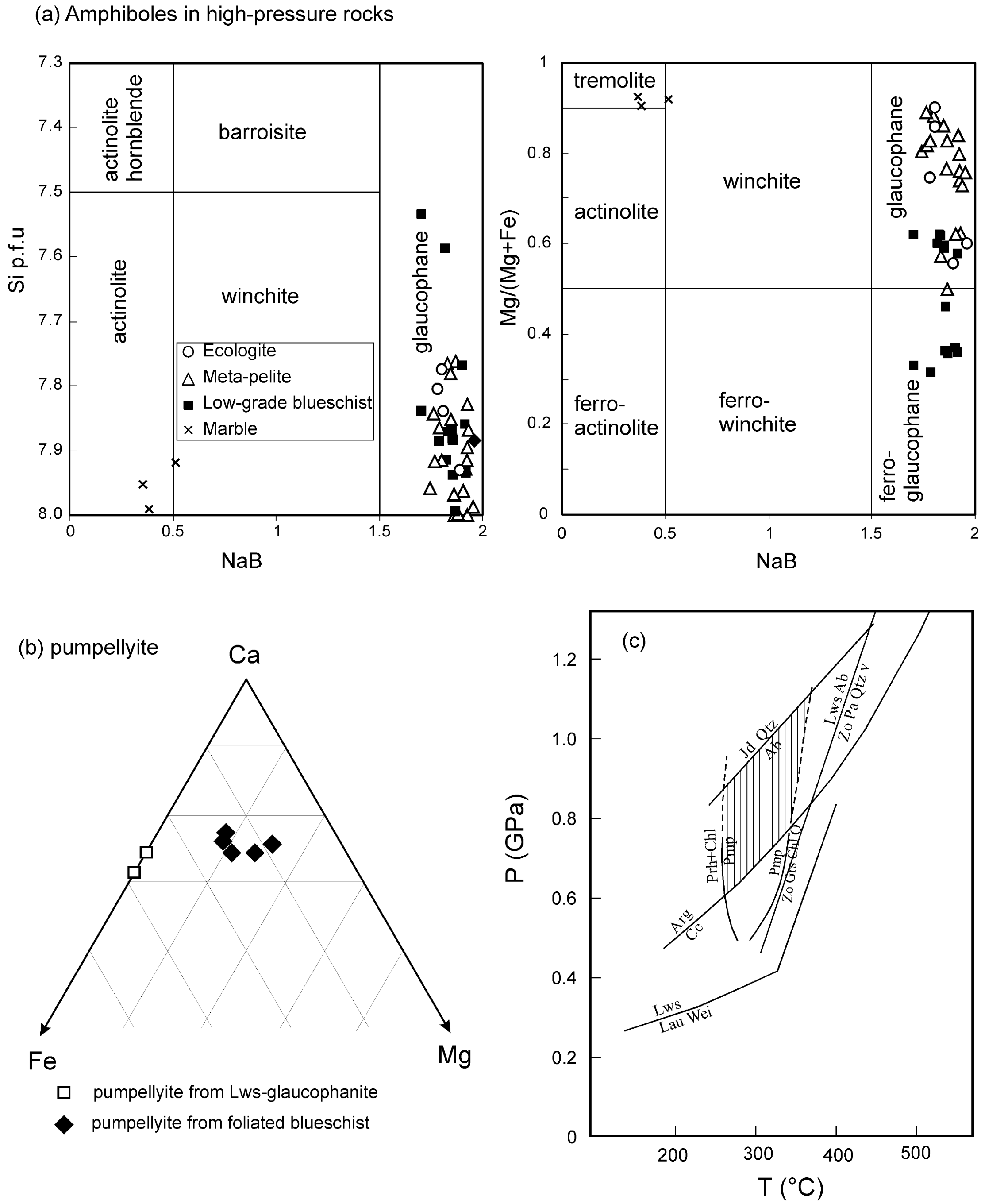


**Fig. 5.** (a) Classification of amphiboles using NaB vs. Si and NaB vs. Mg/(Mg + Fe) diagrams. (b) Ca–Fe–Mg diagram for pumpellyite from low-grade blueschist. (c) *P–T* diagram showing the *P–T* field of low-grade blueschists, reactions Prh + Chl + $H_2O$ = Pmp + Qtz and Pmp = Zo + Grs + Chl + Qtz are after Deer et al. (1992) and other reactions were calculated using Holland and Powell's (1998) THERMORCALC by Okay (2002).

*4.1.3. Eclogite-facies meta-pelites*

Most meta-pelites occur as country rocks or are interlayered with eclogites. Song et al. (2007) reported two kinds of pelitic schist on the basis of their different mineral assemblages. They have also recognized the presence of carpholite (Car), an important index mineral of high-$H_2O$ phase in the cold subduction-zone.

*4.1.3.1. Carpholite-bearing meta-pelite.* Chloritoid–glaucophane schists (Fig. 7e and f) contain four discrete mineral assemblages: (i) Cld–Gln schist with a Cld + Gln + Phn + Ep + Dol + Qtz assemblage without garnet, (ii) Grt–Cld–Gln–Pg schist with a Grt + Cld + Gln + Pg + Ep + Rt + Qtz assemblage, (iii) Car–Cld schist with a Grt + Car + Cld + Phn + Rt + Qtz (±Gln) (Fig. 8d) assemblage, and (iv) Grt–Cld–Gln–Phn schist with a Grt + Cld + Gln + Phn + Ep + Rt + Qtz assemblage (Fig. 8e). The first two types occur mainly in the west part of the high-grade blueschist belt, and the latter two types occur together as a ~200 m-thick layer in the Baijingsi section (Fig. 6b). Wei and Song (2008) reported talc in the chloritoid–glaucophane schists.

Mg-carpholite has been found so far in meta-pelite from the southern part of the Baijingsi cross-section, 30 km east of the town of Qilian (Fig. 6b). The Car–Cld schist mainly consists of Mg-carpholite (15–20%), garnet (~5–8%), Mg-rich chloritoid (~10–15%), phengite (10–15%) and quartz (30–40%) with minor tourmaline.

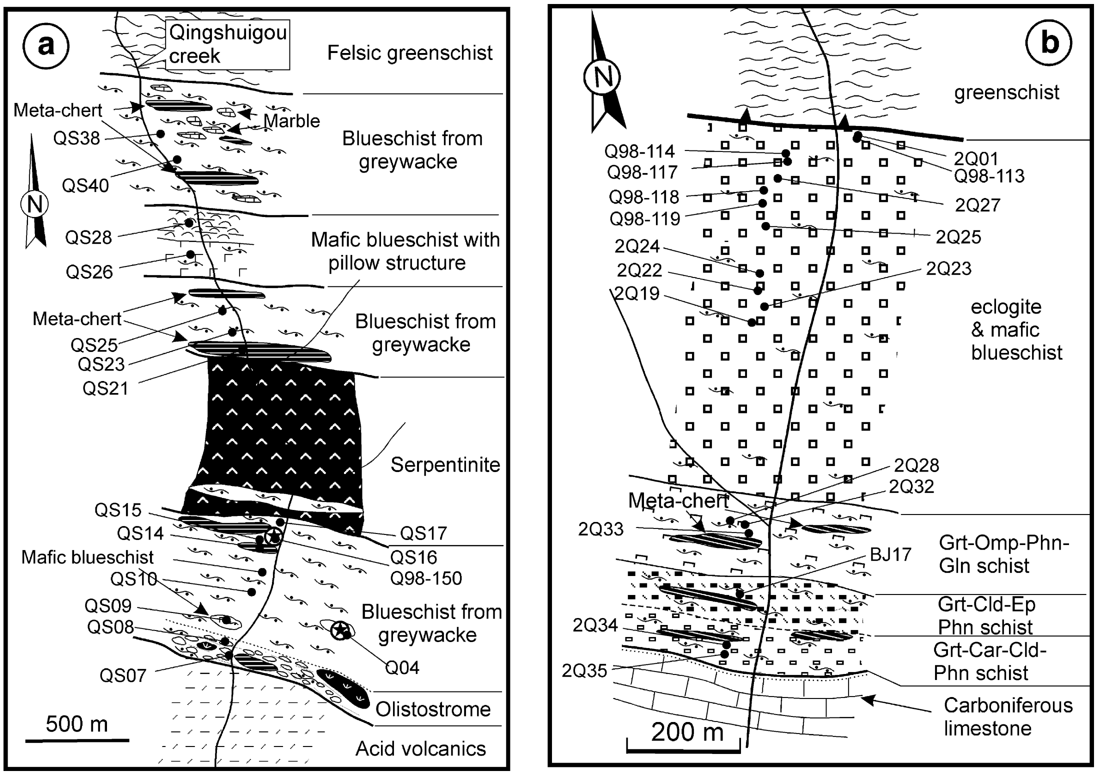


**Fig. 6.** Two representative cross-sections and sample locations of the high-grade blueschist belt. (a) Qingshuigou cross-section and (b) Baijingsi cross-section (see Fig. 2 for localities).

Rare glaucophane grains occur in the matrix, or as inclusions in garnet. Coarse-grained prismatic Mg-carpholite crystals of 0.1–0.4 mm occur in the matrix (Fig. 8d), and as small inclusions in chloritoid. Mg-rich chloritoid occurs as porphyroblastic crystals in equilibrium with Mg-carpholite, garnet and phengite. Some chloritoid crystals are retrogressed into chlorite and pyrophyllite at low *P*–*T* ($T < \sim 400$ °C, Deer et al., 1992) conditions from a reaction chloritoid + quartz + $H_2O$ → pyrophyllite + chlorite. THERMOCALC (Powell et al., 1998) gives equilibrium $T = 520$–$530$ °C and $P = 2.45$–$2.50$ GPa for carpholite-bearing schists (Song et al., 2007).

*4.1.3.2. Garnet–omphacite–phengite–glaucophane (Grt–Omp–Phn–Gln) schist.* The Grt–Omp–Phn–Gln schist occurs as a ~100 m thick layer in the Baijingsi cross-section and is bounded by a large block of eclogite to the north and the Car–Cld schist to the south (Fig. 6b). This schist consists of garnet porphyroblasts set in a foliated fine-grained matrix of omphacite, phengite, glaucophane, rutile, epidote and quartz. The Grt–Omp–Phn geothermobarometer of Ravna and Terry (2004) gives equilibrium $T = 445$–$496$ °C and $P = 2.15$–$2.25$ GPa (Song et al., 2007).

### 4.1.4. Meta-chert

Meta-cherts occur as blocks or layers (~50 m in maximum thickness) enclosed in meta-greywacke and pelitic schists. Most meta-cherts are strongly deformed with isoclinal folds (Fig. 7g). They are dominated by elongate recrystallized quartz with minor phengitic mica; some samples also contain minor garnet and glaucophane. Mn-ore has been exploited in the manganese-bearing meta-chert, suggesting a protolith of pelagic sediment from the ocean floor.

### 4.1.5. Marble

Marble also occurs as blocks of varying size in felsic blueschists. Some marble blocks have banded structure (Fig. 7h) with interbedded layers of Cc + Qtz and Gln + Ep ± sodic Cpx assemblage (Fig. 8f).

## 4.2. Mineral chemistry

### 4.2.1. Garnet

Compositions of garnet from two types of eclogites and pelitic schists are shown in Fig. 9a. Garnet crystals in eclogites have pronounced compositional zoning; from core to rim, spessartine (Sps) decreasing from 19.7 to 0.8 mol%, almandine (Alm) increasing from 45.58 to 60.58 mol% and pyrope (Prp) increasing from 4.5 to 18.0 mol% (Fig. 9b). Garnet zoning in eclogites is also obvious in terms of mineral inclusions; garnet is rich in low-*P* mineral inclusions of zoisite/epidote, quartz and rare albite in the core, and contains high-*P* assemblage of omphacite, phengite, lawsonite and its pseudomorph in the mantle and rim portions.

Garnet crystals from meta-pelites are also compositionally zoned; from core to rim, Sps decreases from 12.43 to 5.16 mol%, and Prp increases from 11.65 to 18.10 mol% (Fig. 9c). Almandine component is also increasing from the core to rim but slightly decreasing in the outermost rim. Grossular component is relatively constant (13.57–16.79 mol%) and lower than garnets from eclogites.

### 4.2.2. Clinopyroxene

All clinopyroxene grains in eclogites and meta-pelitic rocks are sodic and plot in the omphacite field of Morimoto's Augite (WEF)–Jadeite (Jd)–Aegirine (Ae) diagram (Morimoto 1988, Fig. 10). Omphacite in Type-I phengite eclogite varies in a relatively narrow range of $X_{Jd}$ ~0.33–0.47, $X_{Ae}$ ~0.11–0.17 and $X_{Au}$ ~0.46–0.55. Omphacite in Type-II epidote–eclogite, on the other hand, shows wider compositional variations, with the $X_{Jd}$ ranging from 0.28 to 0.54, and $X_{Ae}$ from 0 to 0.25 (Fig. 10).

Sodic clinopyroxene from meta-pelitic rocks in the Baijingsi cross-section (Fig. 6b) contains higher jadeite and aegirine components than mafic eclogites. Sodic clinopyroxene in marbles, however, contains the highest aegirine component ($X_{Ae}$) ranging from 0.61 to 0.79 (Fig. 10).

**Table 3**
Mineral assemblages of blueschist and eclogite in Qingshuigou and Baijingsi cross-sections from the high-grade blueschist belt (see Fig. 6 for sample localities).

| Sample | Rock type | Mineral assemblage |
|---|---|---|
| *Qingshuigou cross-section* | | |
| QS07 | Meta-greywacke | Gln, Phn, Ep, Pl, Qtz |
| QS08 | Marble | Ms, Cc |
| QS09 | Mafic blueschist | Gln, Phn, Ep, Ab, Qtz |
| QS10 | Meta-greywacke | Grt, Gln, Phn, Ep, Qtz, Rt |
| QS11 | Meta-greywacke | Grt, Gln, Phn, Ep, Qtz |
| QS14 | Meta-chert | Gln, Phn, Qtz |
| QS15 | Mafic blueschist | Gln, Phn, Ep, Qtz, Rt |
| QS16 | Retrograde eclogite | Grt, Omp, Gln, Phn, Ep, Qtz, Rt |
| Q98-150 | Retrograde Type-I eclogite | Grt, Omp, Gln, Phn, Ep, Qtz, Rt |
| QS17 | Meta-pelite | Cld, Gln, Phn, Cc, Qtz |
| QS21 | Meta-chert | Gln, Phn, Qtz |
| QS23 | Meta-greywacke | Grt, Gln, Phn, Ep, Qtz, Rt |
| QS25 | Meta-greywacke | Grt, Gln, Phn, Ep, Qtz, Rt |
| QS26 | Mafic blueschist | Gln, Phn, Ep, Chl, Ab |
| QS28 | Mafic blueschist | Gln, Ep, Chl, Ab |
| QS38 | Meta-greywacke | Grt, Gln, Phn, Ep, Qtz, Rt |
| QS40 | Meta-greywacke | Grt, Gln, Phn, Ep, Qtz, Rt |
| Q04 | Phengite eclogite | Grt, Omp, Phn, Gln, Ep, Lws inclusion, Qtz, Rt |
| *Baijingsi cross-section* | | |
| 2Q01 | Epidote eclogite | Grt, Omp, Ep/Cz, Phn, Gln, Rt |
| Q98-113 | Epidote eclogite | Grt, Omp, Ep/Cz, Phn, Gln, Rt |
| Q98-114 | Epidote eclogite | Grt, Omp, Ep/Cz, Phn, Gln, Rt |
| Q98-117 | Epidote eclogite | Grt, Omp, Ep/Cz, Phn, Gln, Rt |
| Q98-118 | Epidote eclogite | Grt, Omp, Ep/Cz, Phn, Gln, Rt |
| Q98-119 | Epidote eclogite | Grt, Omp, Ep/Cz, Phn, Gln, Rt |
| 2Q19 | Epidote eclogite | Grt, Omp, Ep/Cz, Phn, Gln, Qtz |
| 2Q22 | Epidote eclogite | Grt, Omp, Ep/Cz, Phn, Gln, Qtz |
| 2Q23 | Blueschist | Grt, Gln, Phn, Ep, Qtz, Rt |
| 2Q24 | Epidote eclogite | Grt, Omp, Ep/Cz, Phn, Gln, Rt |
| 2Q25 | Epidote eclogite | Grt, Omp, Cz, Phn, Gln, Rt |
| 2Q27 | Epidote eclogite | Grt, Omp, Cz, Phn, Gln, Lws inclusion, Rt |
| 2Q28 | Meta-pelite | Grt, Omp, Ep/Cz, Phn, Gln, Rt |
| 2Q32 | Meta-pelite | Grt, Omp, Ep/Cz, Phn, Gln, Qtz, Rt |
| 2Q33 | Meta-pelite | Grt, Omp, Ep/Cz, Phn, Gln, Qtz, Rt |
| BJ17 | Meta-pelite | Grt, Cld, Gln, Phn, Qtz, Chl, Ep/Cz, Rt |
| 2Q34 | Meta-pelite | Grt, Car, Cld, Gln, Phn, Qtz, Rt, Tur |
| 2Q35 | Meta-pelite | Grt, Car, Cld, Gln, Phn, Qtz, Rt, Tur |

Mineral abbreviations are after Kretz (1983) except for Phn for phengite and Car for carpholite.

*4.2.3. Phengitic mica*

Phengitic micas from the two types of eclogite range in Si content from 3.41 to 3.47 cations per formula unit (p.f.u.) on the basis of 11 oxygens. Phengitic mica from various meta-pelites shows a wide range of compositions (Fig. 11). In garnet-free Cld–Gln schist (QS35), phengite contains relatively lower silica contents (3.36–3.39 p.f.u.) than other meta-pelites. Phengite in Grt–Cld–Gln–Phn schist shows silica contents from 3.38 to 3.41 p.f.u., and, in Car–Cld schist, from 3.44 to 3.51 p.f.u. Phengite from Grt–Omp–Gln–Phn schist has the highest silica content from 3.46 to 3.53 p.f.u.

*4.2.4. Amphibole*

Sodic amphibole is a ubiquitous phase in all rocks in the high-grade blueschist belt. They are almost pure glaucophane with Si > 7.7 and Na/(Na + Ca) > 0.90 (except for amphiboles from marble that plot in tremolite field in Fig. 5a). Most glaucophanes, from both mafic eclogites and meta-pelites, all show clear compositional zoning with higher Mg/(Mg + $Fe^{2+}$) and $Fe^{3+}$/($Fe^{3+}$ + Al) ratios towards the rim.

*4.2.5. Mg-carpholite*

Carpholite in metapelitic schists is characterized by high-Mg content with $X_{Mg}$ [Mg/(Mg + $Fe^{2+}$ + Mn)] ranging from 0.73 to 0.87, $X_{Fe}$ from 0.13 to 0.27, and $X_{Mn}$ from 0.000 to 0.002 (Song et al., 2007).

*4.2.6. Chloritoid*

Chloritoid in various chloritoid-bearing schists differs in Mg/(Mg + Fe) ratios ranging from 0.17 to 0.55. Chloritoids from carpholite-bearing schists have the highest MgO content (Mg/(Mg + Fe) = 0.46–0.55).

## 5. Chemical compositions of blueschists and eclogites

Whole-rock major element analyses for eclogites were performed on a Perkin Elmer Optima 3300 DV ICP-OES at University of Queensland (Niu, 2004) and X-ray fluorescence (XRF) at Northwest University, Xi'an, China (Rudnick et al., 2004). Trace elements analyses were made using a Fisons PQ2 ICP-MS at University of Queensland, Australia (e.g., Niu and Batiza, 1997) and an Elan 6100-DRC ICP-MS at Northwest University, Xi'an, China (e.g., Rudnick et al., 2004). For major elements, precision (RSD) is better than 6% and accuracy is better than 4%; for trace elements, precision is generally better than 5% for most elements and accuracy is better than 10%, with many elements agreeing to within 2% of the reference values. Major and trace elements of representative eclogite and mafic blueschist samples from both low-grade and high-grade blueschist belts are given in Table 4.

*5.1. Chemical compositions of low-grade blueschists*

On the basis of whole-rock composition, the ophiolitic complex north of the low-grade blueschist belt was interpreted as probably having formed in a back-arc spreading centre (Feng and He, 1995; Qian et al., 2001; Xia et al., 2003). The rock assemblages, especially the cumulate with banded wehrlite + gabbro and high volume of

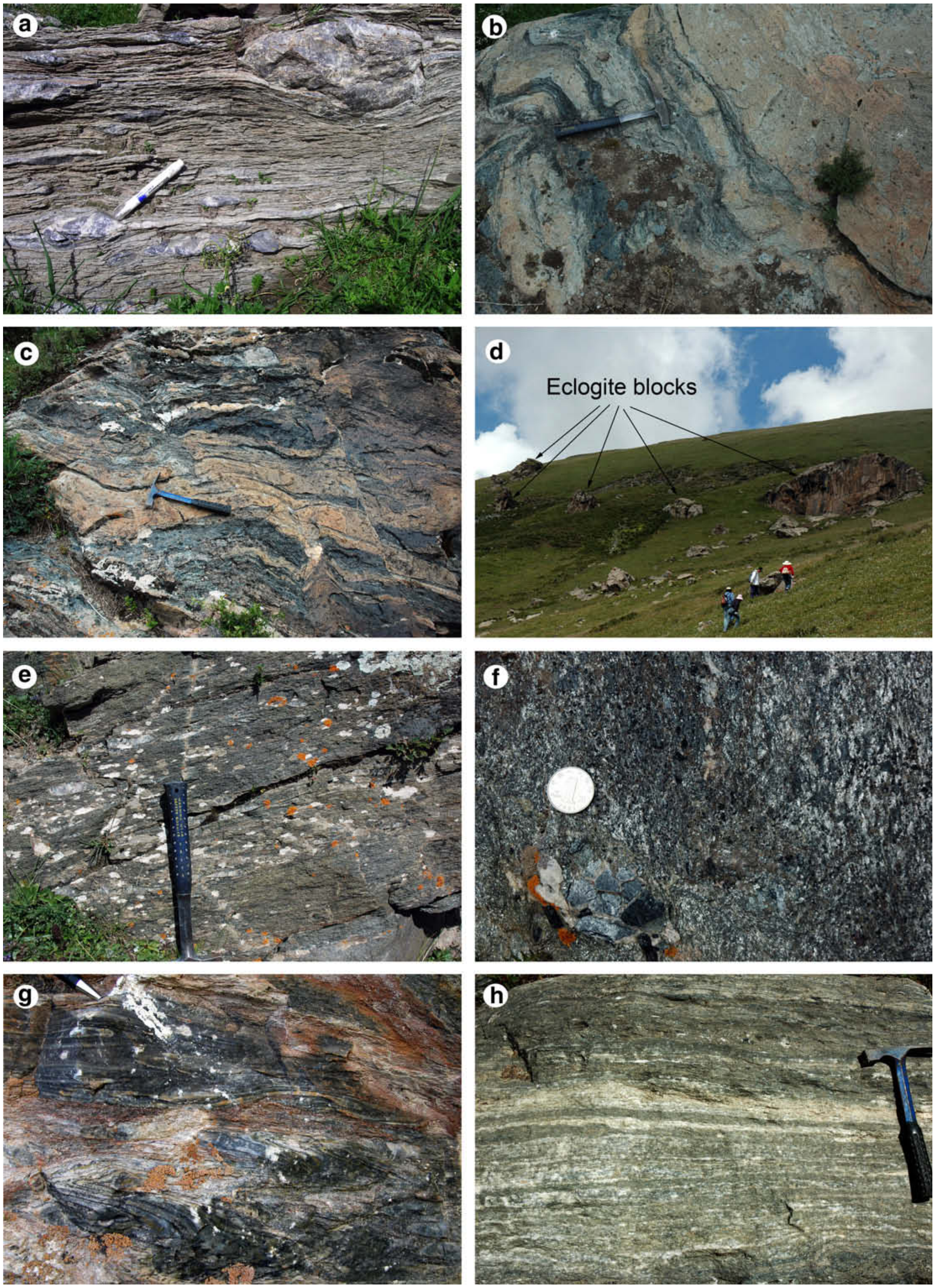


**Fig. 7.** Photographs of various rocks in the high-grade blueschist belt. (a) Strongly deformed oliststrome in the Qishuigou cross-section. (b) and (c) Blueschist-facies metamorphosed turbidite with interbedded sandstone and mud layers. (d) Eclogite blocks within meta-pelite. (e) Mg-carpholite-bearing meta-pelite in the Baijingsi cross-section. (f) Grt–Cld–Gln–Phn schist in the west of the Baijingsi cross-section. (g) Strongly deformed meta-chert in the Qingshuigou cross-section. (h) Marble with banded structure in the west of the Qingshuigou cross-section.

volcanic breccias suggest that the ophiolite complex may be a supra-subduction-zone (SSZ) type.

Three samples, Q98-34 (massive lawsonite–glaucophanite), Q98-35 (schistose lawsonite-bearing blueschist) and Q98-40 (relict Cpx-bearing blueschist), were chosen for analysis. These analyses show protoliths of tholeiitic basalt with $SiO_2 < 50$ wt%, $TiO_2$ 1.12–1.49 wt%, and relatively high MgO (7.0–9.6 wt%) and low to medium $K_2O$ content (0.16–1.1 wt%); all plot in the sub-alkaline basalt field in the TAS diagram of Le Bas et al. (1986; Fig. 12). The chondrite-normalized (Sun and McDonough, 1989) rare earth element (REE) patterns indicate their resemblance to N-type MORB (Fig. 13a). In the primitive mantle normalized (Sun and McDonough, 1989) multi-element diagram (Fig. 13b), these three rocks show patterns consistent with N-type MORB except for the enrich-

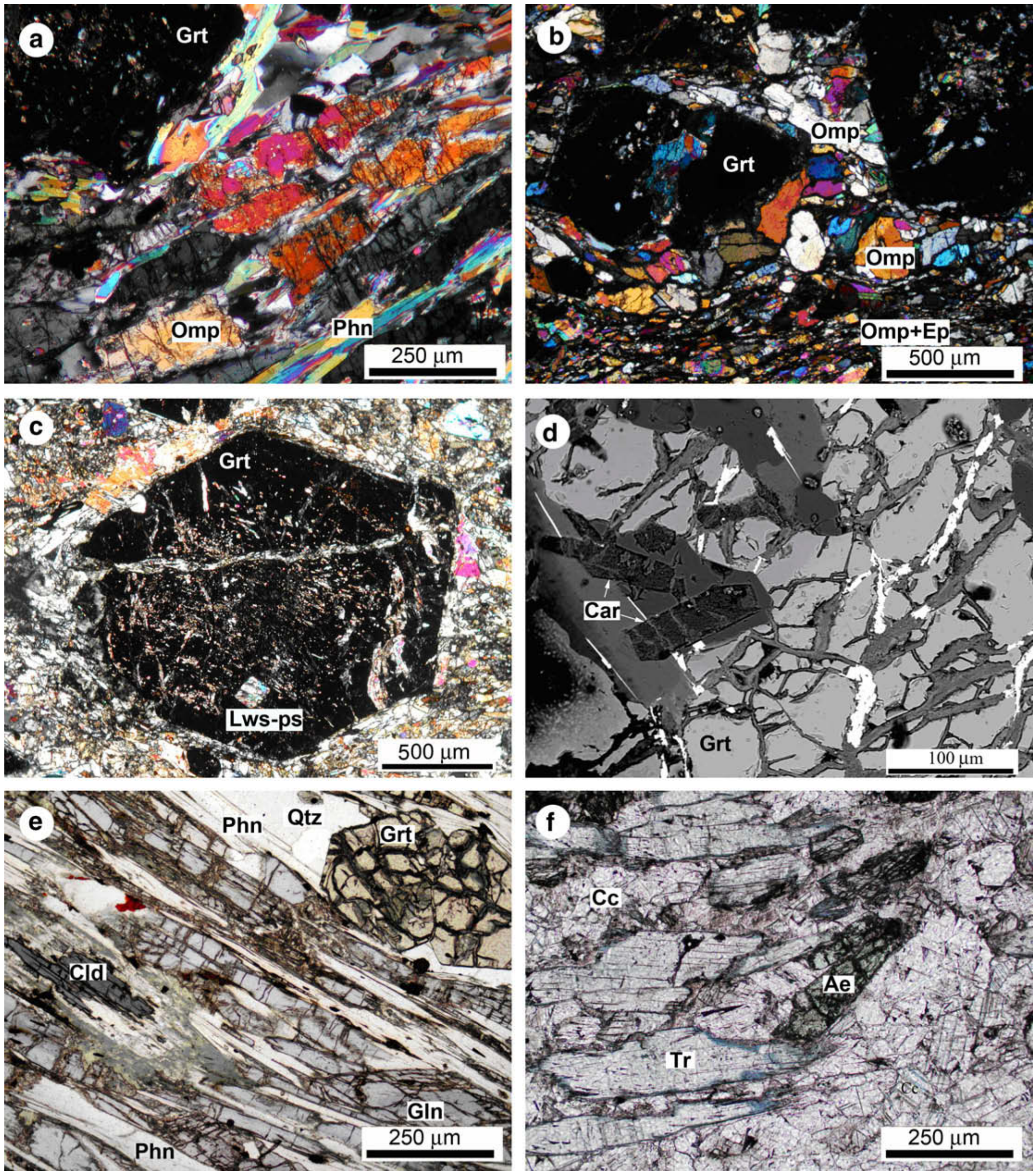


**Fig. 8.** Photomicrographs of various eclogite-facies metamorphic rocks in the high-grade blueschist belt. (a) Phengite eclogite with assemblage of Grt + Omp + Phn + Rt (cross-polarized light). (b) Epidote eclogite showing that foliated Omp+Ep overprinting the early stage of Grt + Omp (cross-polarized light). (c) Porphyroblastic garnet with a large number of inclusion and lawsonite pseudomorph (Lws-Ps) (cross-polarized light). (d) Back-scattered image showing euhedral carpholite crystals coexisting with garnet. (e) Grt–Cld–Gln–Phn schist (plane polarized light). (f) Aegirine–tremolite marble with Tr + Ae + Cc assemblage (plane polarized light).

ment of fluid-mobile large ion lithospheric elements (LILE) such as Cs, Rb, Ba, U and to a lesser extent Th. In trace element discrimination diagrams, e.g., Zr vs. Zr/Y (Pearce and Norry, 1979) and Nb–Zr–Y (Meschede, 1986), they are all plotted in the MORB field (Fig. 14). All these suggest that REE and high field strength elements (HFSE) such as Nb and Zr have experienced no significant change during HP metamorphism.

### *5.2. Chemical compositions of eclogites in the high-grade blueschist belt*

Phengite-rich eclogites have variable $SiO_2$ from 44 to 55 wt%, relatively high $K_2O$ ($K_2O$ > 2.0 wt%), and high but variable $TiO_2$ (1.15–2.98 wt%) (Table 4). In the TAS diagram (Le Bas et al., 1986; Fig. 12), most samples plot in the alkaline fields of tephrite basanite, trachybasalt and basaltic trachyandesite and two samples plot in the sub-alkaline basalt field.

The chondrite-normalized REE patterns of phengite eclogites show strong LREE enrichment and flat to moderate HREE depletion ($La_N/Sm_N$ = 3–25), which differ significantly from the low-grade blueschists and epidote eclogites (Fig. 13c). In the primitive mantle (PM) normalized multi-element diagram (Fig. 13d), phengite eclogites show patterns similar to present-day E-type MORB and ocean island basalts (OIB). While these samples may plot in the fields of MORB and intraplate settings in the Zr vs. Zr/Y (Pearce and Norry, 1979) and Nb–Zr–Y discrimination diagrams, modern seafloor petrology and geochemistry suggest that the protoliths of phengite eclogites are most like E-type MORB or alkali basalts from ridges and near ridge seamounts (Batiza et al., 1989, 1990; Niu and Batiza, 1997) without ruling out the possibility of an OIB protolith.

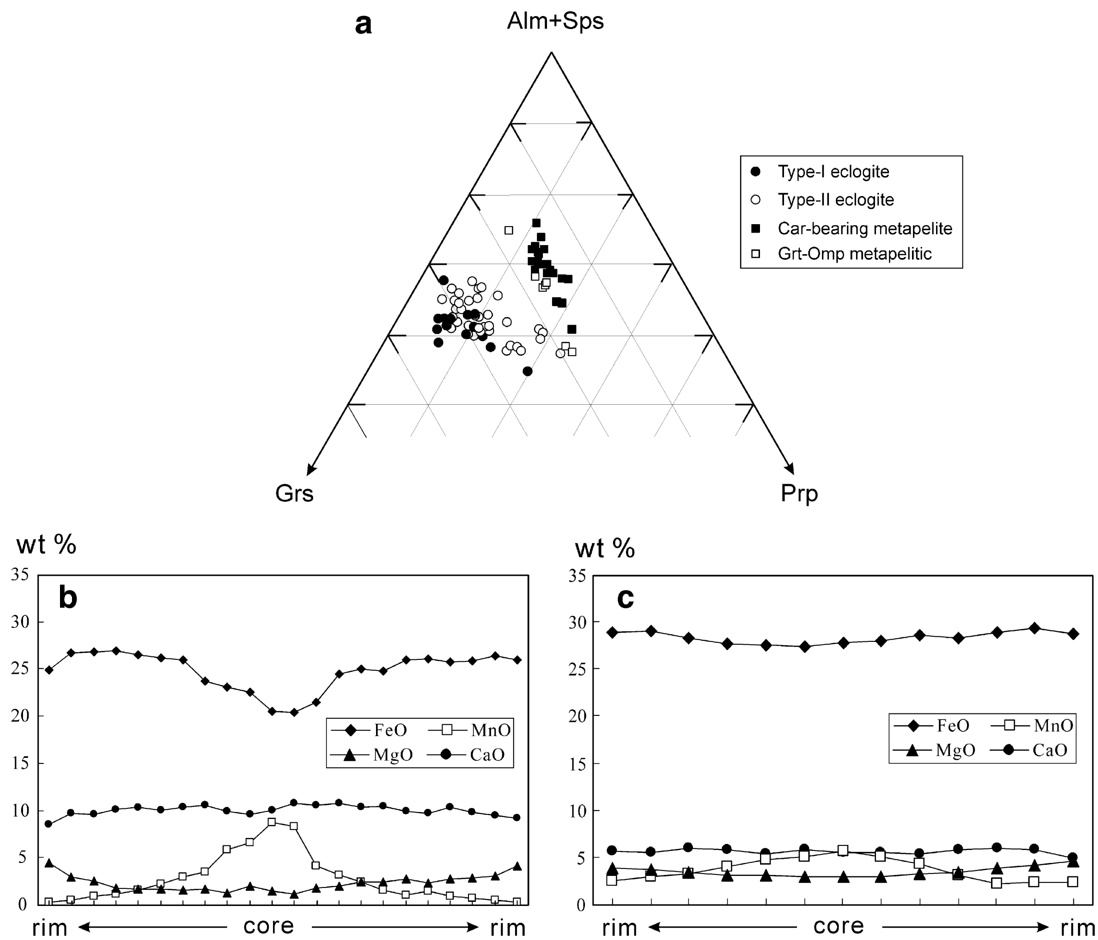


**Fig. 9.** (a) Diagram showing compositional variation of garnet from eclogites and meta-pelites. (b) Compositional profile of a lawsonite-bearing garnet from eclogite. (c) Compositional profile of garnet from Mg-carpholite-bearing meta-pelite.

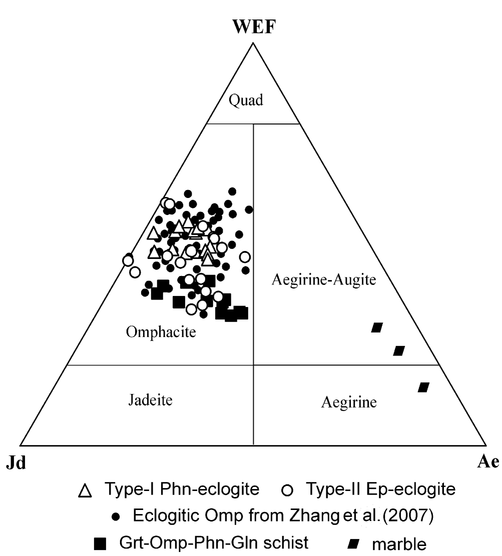


**Fig. 10.** Jd–Ae–WEF ternary diagram showing sodic clinopyroxene compositions from eclogites, meta-pelite and marble.

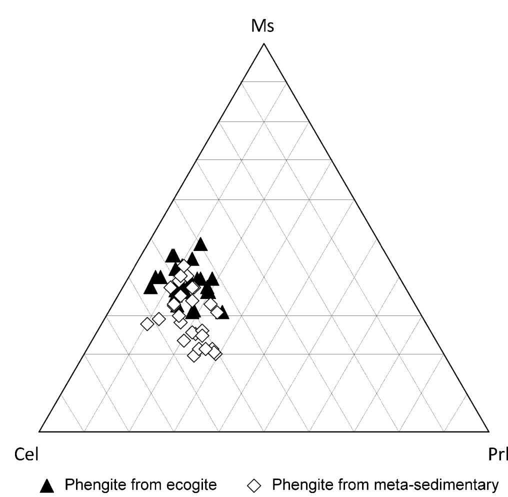


**Fig. 11.** Ms–Cel–Prl ternary diagram showing compositional variation of phengitic mica from eclogite and meta-sedimentary rocks.

In contrast, epidote-rich eclogites have relatively low $K_2O$ (0.37–1.56 wt%) and variable $TiO_2$ (0.71–2.15 wt%) and $Al_2O_3$ (14.64–20.83 wt%). Most samples plot within the sub-alkaline basalt field in the TAS diagram and only one in the basaltic trachy-andesite field (Fig. 12).

On the basis of chondrite-normalized REE patterns, protoliths of epidote eclogite can be further subdivided into two groups: the N- to E-type MORB group and the gabbroic group. The N- to E-type MORB group samples (Fig. 13e and f) show flat or slightly LREE-enriched patterns ($La_N/Sm_N = 0.84–2.53$ and $La_N/Yb_N = 0.89–4.17$) without Eu anomaly ($Eu/Eu^* = 0.94–1.03$). The primitive mantle (PM) normalized multi-element diagram displays similar patterns

**Table 4**
Whole-rock compositions of mafic low-grade blueschists and eclogites in the North Qilian suture zone.

| Sample | Low-grade blueschist | | | Type I phengite-rich ecloigte in high-grade blueschist belt | | | | | | | |
|---|---|---|---|---|---|---|---|---|---|---|---|
| | Q98-34 | Q98-35 | Q98-40 | Q98-116 | Q98-133 | Q98-135 | Q98-150 | Q03[a] | Q78 [a] | Q35 [a] | Q67 [a] |
| Location | Tadungou | Tadungou | Tadungou | Baijingsi | Qinshuigou | Qinshuigou | Qinshuigou | Qinshuigou | Qinshuigou | Xiangzigou | Xiangzigou |
| $SiO_2$ | 48.08 | 48.91 | 49.07 | 48.33 | 44.32 | 52.20 | 54.02 | 51.98 | 49.56 | 46.83 | 45.43 |
| $TiO_2$ | 1.22 | 1.17 | 1.49 | 1.15 | 2.34 | 2.02 | 1.25 | 2.29 | 2.87 | 2.05 | 2.98 |
| $Al_2O_3$ | 18.09 | 17.67 | 15.70 | 18.01 | 20.95 | 14.81 | 16.69 | 13.65 | 14.50 | 14.62 | 16.15 |
| FeOt | 10.98 | 9.91 | 10.58 | 8.41 | 13.48 | 14.01 | 13.31 | 15.01 | 11.72 | 15.87 | 12.19 |
| MnO | 0.23 | 0.28 | 0.18 | 0.17 | 0.09 | 0.15 | 0.27 | 0.18 | 0.18 | 0.26 | 0.15 |
| MgO | 9.10 | 9.67 | 7.03 | 7.80 | 3.72 | 5.77 | 4.72 | 5.43 | 6.58 | 5.13 | 4.71 |
| CaO | 4.27 | 4.85 | 6.22 | 8.85 | 1.80 | 2.47 | 3.33 | 3.90 | 6.19 | 6.74 | 7.52 |
| $Na_2O$ | 2.91 | 2.55 | 3.66 | 1.69 | 2.96 | 2.59 | 1.95 | 3.60 | 2.95 | 2.24 | 2.47 |
| $K_2O$ | 0.79 | 1.16 | 0.17 | 2.25 | 5.47 | 4.32 | 3.71 | 1.42 | 2.94 | 2.18 | 3.40 |
| $P_2O_5$ | 0.15 | 0.19 | 0.19 | 0.22 | 1.51 | 0.35 | 0.34 | 0.22 | 0.52 | 0.30 | 0.68 |
| LOI | | | | | | | | 1.55 | 2.44 | 4.31 | 3.44 |
| Total | 95.85 | 96.37 | 94.30 | 96.88 | 96.65 | 98.69 | 99.60 | 99.23 | 100.45 | 100.53 | 99.12 |
| ppm | | | | | | | | | | | |
| Li | 44.4 | 35.1 | 12.1 | 20.9 | 45.9 | 25.9 | 52.4 | | | | |
| Be | 0.32 | 0.43 | 0.59 | 0.83 | 3.19 | 1.49 | 0.90 | | | | |
| Sc | 36.0 | 37.9 | 41.8 | 30.1 | 31.8 | 34.7 | 24.2 | 43.3 | 20.3 | 45.3 | 25.7 |
| V | 270.7 | 229.0 | 260.1 | 201.2 | 172.7 | 315.9 | 159.9 | 522.5 | 196.1 | 248.7 | 258.0 |
| Cr | 400.1 | 354.4 | 157.4 | 327.4 | 176.2 | 65.6 | 146.8 | 30 | 165 | 208 | 68 |
| Co | 47.2 | 44.2 | 53.7 | 42.6 | 34.3 | 42.1 | 23.4 | 30.1 | 30.9 | 41.9 | 42.8 |
| Ni | 130.1 | 90.0 | 66.4 | 122.1 | 65.7 | 62.3 | 69.0 | 64 | 120 | 142 | 69 |
| Cu | 57.0 | 205.7 | 57.5 | 52.2 | 23.7 | 70.5 | 66.8 | | | | |
| Zn | 80.8 | 70.0 | 71.7 | 76.8 | 125.8 | 89.8 | 74.5 | | | | |
| Ga | 16.6 | 14.8 | 14.4 | 16.8 | 24.2 | 18.6 | 16.5 | | | | |
| Rb | 14.0 | 18.5 | 1.17 | 37.6 | 85.3 | 72.0 | 46.3 | 29 | 22 | 52 | 92 |
| Sr | 77.0 | 75.4 | 68.0 | 372.2 | 154.4 | 89.7 | 168.7 | 171.3 | 147.9 | 56.86 | 140.1 |
| Y | 21.86 | 24.86 | 29.58 | 20.14 | 27.37 | 35.87 | 31.73 | 42.45 | 12.18 | 35.35 | 20.15 |
| Zr | 60.8 | 83.1 | 96.2 | 79.2 | 356.6 | 173.4 | 170.2 | 157 | 159 | 163 | 117 |
| Nb | 1.33 | 2.21 | 3.04 | 8.88 | 92.89 | 14.25 | 15.26 | 15.1 | 88 | 26 | 10 |
| Sn | 0.76 | 0.79 | 1.05 | 1.20 | 3.65 | 2.73 | 2.65 | | | | |
| Cs | 3.44 | 2.19 | 0.35 | 1.04 | 3.65 | 2.86 | 2.70 | | | | |
| Ba | 125.0 | 88.7 | 25.2 | 389.9 | 1301 | 1045 | 265.9 | 457.8 | 289 | 672.4 | 1238 |
| La | 2.17 | 3.52 | 3.52 | 10.72 | 87.38 | 19.84 | 16.91 | 20.08 | 31.79 | 21.27 | 34.9 |
| Ce | 7.05 | 10.24 | 10.81 | 23.80 | 183.59 | 46.97 | 39.11 | 45.22 | 63.57 | 46.29 | 73.34 |
| Pr | 1.28 | 1.69 | 1.85 | 3.10 | 21.87 | 5.94 | 4.86 | 5.709 | 7.062 | 4.785 | 7.15 |
| Nd | 6.90 | 8.50 | 9.47 | 12.70 | 77.42 | 23.86 | 18.28 | 26.65 | 28.95 | 21.34 | 29.63 |
| Sm | 2.45 | 2.77 | 3.22 | 3.16 | 12.64 | 5.95 | 4.25 | 6.98 | 6.64 | 5.11 | 6.24 |
| Eu | 0.91 | 1.13 | 1.16 | 1.12 | 3.38 | 1.62 | 1.22 | 2.11 | 2.01 | 1.71 | 2.21 |
| Gd | 3.38 | 3.61 | 4.43 | 3.73 | 8.72 | 6.36 | 4.56 | 8.424 | 5.751 | 6.435 | 6.048 |
| Tb | 0.60 | 0.65 | 0.80 | 0.63 | 1.13 | 1.08 | 0.82 | 1.46 | 0.62 | 1.09 | 0.85 |
| Dy | 4.11 | 4.41 | 5.41 | 4.00 | 6.10 | 6.92 | 5.57 | 8.32 | 3.11 | 6.88 | 4.27 |
| Ho | 0.89 | 0.97 | 1.16 | 0.81 | 1.13 | 1.43 | 1.23 | 1.78 | 0.67 | 1.45 | 0.9 |
| Er | 2.59 | 2.87 | 3.33 | 2.23 | 2.91 | 4.01 | 3.74 | 4.83 | 1.71 | 3.77 | 2.18 |
| Tm | 0.39 | 0.42 | 0.49 | 0.33 | 0.41 | 0.59 | 0.58 | 0.69 | 0.23 | 0.54 | 0.28 |
| Yb | 2.50 | 2.71 | 3.10 | 2.07 | 2.50 | 3.71 | 3.98 | 4.37 | 1.31 | 3.69 | 1.89 |
| Lu | 0.38 | 0.41 | 0.48 | 0.31 | 0.38 | 0.56 | 0.65 | 0.675 | 0.18 | 0.549 | 0.279 |
| Hf | 1.85 | 2.20 | 2.56 | 2.08 | 8.40 | 4.75 | 4.29 | 5.4 | 4.3 | 4.7 | 3.3 |
| Ta | 0.09 | 0.14 | 0.20 | 0.52 | 4.94 | 0.87 | 0.94 | 0.8 | 5.4 | 3.5 | 1.1 |
| W | 0.22 | 0.44 | 0.73 | 0.39 | 2.64 | 1.46 | 0.84 | | | | |
| Pb | 0.71 | 0.48 | 0.63 | 13.57 | 6.34 | 4.11 | 11.87 | | | | |
| Th | 0.12 | 0.42 | 0.53 | 1.83 | 16.57 | 5.29 | 5.97 | 3.1 | 4.2 | 3.7 | 9.6 |
| U | 0.09 | 0.17 | 0.20 | 0.50 | 3.84 | 1.20 | 1.54 | 1.3 | 2.1 | 0.7 | 2.9 |

| | Type II Epidote-rich eclogite in high-grade blueschist belt | | | | | | | | | | | | | |
|---|---|---|---|---|---|---|---|---|---|---|---|---|---|---|
| Sample ID | Q26[a] | Q58[a] | Q59[a] | Q54[a] | Q98-113 | Q98-114 | Q98-117 | Q98-118 | Q98-119 | Q98-125 | Q98-126 | Q98-127 | Q98-128 | Q98-149 |
| Location | Eclogite | Eclogite | Eclogite | Baijingsi | Baijingsi | Baijingsi | Baijingsi | Baijingsi | Baijingsi | Baijingsi | Baijingsi | Baijingsi | Baijingsi | Qinshuigou |
| *Major elements (wt%)* | | | | | | | | | | | | | | |
| $SiO_2$ | 51.54 | 47.22 | 51.64 | 49.92 | 48.267 | 47.04 | 46.96 | 49.42 | 47.93 | 49.22 | 47.99 | 48.16 | 45.78 | 47.76 |
| $TiO_2$ | 0.90 | 0.88 | 0.64 | 1.49 | 0.708 | 0.90 | 0.90 | 0.82 | 2.15 | 1.59 | 1.64 | 1.73 | 1.56 | 2.07 |
| $Al_2O_3$ | 15.63 | 14.70 | 16.77 | 15.37 | 20.825 | 17.22 | 17.55 | 17.19 | 18.10 | 18.61 | 15.87 | 16.81 | 16.14 | 14.64 |
| FeOt | 11.00 | 8.16 | 6.38 | 10.68 | 8.305 | 8.62 | 8.34 | 8.68 | 14.57 | 11.35 | 10.91 | 14.82 | 12.19 | 15.19 |
| MnO | 0.11 | 0.14 | 0.12 | 0.18 | 0.244 | 0.18 | 0.17 | 0.25 | 0.22 | 0.18 | 0.21 | 0.37 | 0.20 | 0.31 |
| MgO | 6.27 | 8.48 | 9.33 | 6.21 | 7.039 | 8.29 | 7.84 | 8.49 | 4.88 | 5.57 | 6.63 | 7.27 | 7.15 | 7.06 |
| CaO | 9.68 | 11.52 | 5.28 | 8.56 | 8.288 | 8.77 | 9.06 | 7.38 | 8.68 | 7.74 | 8.61 | 6.75 | 7.95 | 7.08 |
| $Na_2O$ | 3.33 | 3.14 | 4.54 | 4.44 | 2.368 | 2.90 | 2.91 | 2.70 | 2.06 | 2.87 | 2.80 | 2.45 | 1.80 | 2.78 |
| $K_2O$ | 0.08 | 0.37 | 0.90 | 0.20 | 1.565 | 0.46 | 0.62 | 1.12 | 0.77 | 1.11 | 1.15 | 1.35 | 1.00 | 0.37 |
| $P_2O_5$ | 0.10 | 0.13 | 0.09 | 0.16 | 0.111 | 0.13 | 0.20 | 0.18 | 0.21 | 0.20 | 0.25 | 0.43 | 0.25 | 0.20 |
| LOI | 1.19 | 4.58 | 3.84 | 2.49 | | | | | | | | | | |
| Total | 99.83 | 99.32 | 99.53 | 99.70 | 97.720 | 94.52 | 94.55 | 96.23 | 99.59 | 98.45 | 96.06 | 100.15 | 94.00 | 97.46 |

(*continued on next page*)

**Table 4** (*continued*)

| | Type II Epidote-rich eclogite in high-grade blueschist belt | | | | | | | | | | | | | |
|---|---|---|---|---|---|---|---|---|---|---|---|---|---|---|
| Sample ID | Q26[a] | Q58[a] | Q59[a] | Q54[a] | Q98-113 | Q98-114 | Q98-117 | Q98-118 | Q98-119 | Q98-125 | Q98-126 | Q98-127 | Q98-128 | Q98-149 |
| Location | Eclogite | Eclogite | Eclogite | Baijingsi | Baijingsi | Baijingsi | Baijingsi | Baijingsi | Baijingsi | Baijingsi | Baijingsi | Baijingsi | Baijingsi | Qinshuigou |
| *Trace elements (ppm)* | | | | | | | | | | | | | | |
| Li | | | | | 33.80 | 33.09 | 35.40 | 40.03 | 16.45 | 16.05 | 20.87 | 36.11 | 42.75 | 27.81 |
| Sc | 32.67 | 31.99 | 26.66 | 35 | 24.22 | 29.11 | 30.30 | 28.73 | 39.64 | 36.64 | 33.95 | 40.37 | 38.20 | 41.86 |
| V | 210.8 | 229.8 | 151.3 | 237.2 | 195.53 | 187.62 | 190.11 | 198.61 | 268.70 | 213.48 | 218.75 | 228.97 | 247.94 | 442.64 |
| Cr | 202 | 427 | 274 | 199 | 299.42 | 446.42 | 444.27 | 313.27 | 218.57 | 315.50 | 277.61 | 284.50 | 162.38 | 95.89 |
| Co | 35.51 | 31.31 | 27.49 | 35.45 | 39.35 | 63.74 | 38.31 | 34.75 | 36.06 | 40.92 | 43.89 | 40.95 | 41.21 | 46.56 |
| Ni | 59 | 185 | 105 | 94 | 81.31 | 168.87 | 141.59 | 90.33 | 62.93 | 97.73 | 115.69 | 114.78 | 56.26 | 46.10 |
| Cu | | | | | 59.14 | 125.72 | 57.30 | 674.12 | 26.05 | 47.91 | 52.76 | 80.35 | 51.71 | 57.14 |
| Zn | | | | | 107.56 | 95.96 | 54.59 | 131.87 | 67.28 | 77.94 | 81.95 | 106.84 | 76.29 | 79.98 |
| Ga | | | | | 19.44 | 14.55 | 13.89 | 14.95 | 19.54 | 17.27 | 14.78 | 14.78 | 15.58 | 16.62 |
| Rb | 2.6 | 8.3 | 22 | 4.4 | 28.18 | 6.07 | 8.50 | 20.93 | 12.92 | 15.14 | 17.32 | 19.38 | 22.18 | 2.97 |
| Sr | 291.6 | 315.3 | 125.1 | 124.7 | 352.94 | 256.62 | 215.48 | 210.63 | 224.48 | 205.70 | 124.15 | 176.43 | 301.09 | 183.06 |
| Y | 18.61 | 15.62 | 10.99 | 26.56 | 14.92 | 18.46 | 18.90 | 17.84 | 38.36 | 28.18 | 29.32 | 35.99 | 30.97 | 35.04 |
| Zr | 54 | 46 | 40 | 110 | 52.55 | 54.62 | 57.72 | 64.21 | 144.54 | 105.26 | 116.02 | 114.69 | 102.63 | 99.23 |
| Nb | 2.6 | 1.6 | 2.2 | 2.6 | 3.53 | 4.47 | 2.73 | 4.31 | 5.04 | 3.40 | 4.15 | 4.60 | 3.95 | 4.06 |
| Sn | | | | | 1.20 | 0.76 | 0.69 | 1.01 | 1.76 | 1.22 | 1.33 | 1.31 | 1.17 | 1.15 |
| Cs | | | | | 1.11 | 0.19 | 0.20 | 0.67 | 1.08 | 1.08 | 1.74 | 1.48 | 1.40 | 0.16 |
| Ba | 12.94 | 100.4 | 183.8 | 42.97 | 259.46 | 66.63 | 78.65 | 167.87 | 62.76 | 89.38 | 87.80 | 152.37 | 261.90 | 47.76 |
| La | 6.05 | 4.32 | 4.24 | 5.7 | 9.45 | 5.98 | 4.78 | 10.61 | 7.34 | 4.60 | 4.90 | 7.61 | 7.12 | 4.66 |
| Ce | 12.97 | 8.18 | 9.63 | 16.34 | 19.89 | 13.90 | 12.07 | 22.85 | 20.79 | 14.15 | 15.18 | 18.39 | 18.24 | 13.20 |
| Pr | 1.925 | 1.43 | 1.166 | 2.013 | 2.50 | 1.90 | 1.77 | 2.88 | 3.51 | 2.28 | 2.49 | 2.64 | 2.68 | 2.15 |
| Nd | 9.43 | 5.69 | 4.6 | 11.44 | 10.09 | 8.27 | 8.05 | 11.35 | 17.22 | 11.23 | 11.99 | 11.87 | 12.39 | 10.38 |
| Sm | 2.69 | 2.2 | 1.32 | 3.49 | 2.41 | 2.28 | 2.37 | 2.71 | 5.28 | 3.51 | 3.69 | 3.43 | 3.66 | 3.59 |
| Eu | 1.23 | 1.12 | 0.59 | 1.37 | 1.21 | 0.85 | 0.87 | 0.97 | 1.95 | 1.34 | 1.32 | 1.23 | 1.29 | 1.27 |
| Gd | 3.321 | 2.781 | 1.638 | 4.014 | 2.88 | 2.87 | 3.09 | 3.15 | 6.56 | 4.47 | 4.67 | 4.60 | 4.80 | 4.79 |
| Tb | 0.54 | 0.44 | 0.31 | 0.73 | 0.48 | 0.50 | 0.54 | 0.53 | 1.13 | 0.79 | 0.82 | 0.87 | 0.84 | 0.89 |
| Dy | 3.55 | 3 | 2.03 | 4.85 | 2.87 | 3.35 | 3.55 | 3.36 | 7.33 | 5.21 | 5.31 | 6.06 | 5.62 | 6.19 |
| Ho | 0.83 | 0.62 | 0.49 | 1.06 | 0.59 | 0.74 | 0.77 | 0.71 | 1.53 | 1.13 | 1.18 | 1.44 | 1.25 | 1.35 |
| Er | 2.29 | 1.92 | 1.28 | 3 | 1.73 | 2.15 | 2.17 | 1.98 | 4.35 | 3.24 | 3.43 | 4.41 | 3.70 | 3.97 |
| Tm | 0.33 | 0.28 | 0.18 | 0.44 | 0.27 | 0.33 | 0.31 | 0.29 | 0.64 | 0.47 | 0.50 | 0.68 | 0.58 | 0.59 |
| Yb | 2.15 | 1.81 | 1.26 | 3 | 1.75 | 2.10 | 1.98 | 1.82 | 4.00 | 2.99 | 3.14 | 4.40 | 3.79 | 3.78 |
| Lu | 0.324 | 0.261 | 0.18 | 0.441 | 0.27 | 0.32 | 0.30 | 0.27 | 0.61 | 0.45 | 0.46 | 0.68 | 0.57 | 0.58 |
| Hf | 2.1 | 1.5 | 1.2 | 2.9 | 1.48 | 1.53 | 1.60 | 1.76 | 3.65 | 2.63 | 2.91 | 3.08 | 2.73 | 2.83 |
| Ta | 0.2 | 0.1 | 0.2 | 0.2 | 0.22 | 0.25 | 0.14 | 0.24 | 0.33 | 0.22 | 0.27 | 0.27 | 0.23 | 0.27 |
| W | | | | | 0.16 | 0.17 | 0.22 | 0.18 | 0.54 | 0.23 | 0.08 | 0.77 | 1.17 | 1.48 |
| Pb | | | | | 6.72 | 4.85 | 2.96 | 3.50 | 6.51 | 2.17 | 0.73 | 8.60 | 25.36 | 3.22 |
| Th | 1.1 | 0.6 | 0.8 | 0.5 | 2.13 | 1.01 | 0.64 | 2.30 | 0.38 | 0.27 | 0.34 | 1.18 | 1.02 | 0.68 |
| U | 0.4 | 0.2 | 0.2 | 0.2 | 0.61 | 0.32 | 0.17 | 0.56 | 0.14 | 0.10 | 0.11 | 0.50 | 0.31 | 0.19 |

[a] Samples were analysed by XRF for major elements and ICP-MS for trace elements at Northwest University, China. Others were analysed by ICP-OES for major elements and ICP-MS for trace elements at The University of Queensland, Australia.

to N- to E-type MORB (e.g., Sun and McDonough, 1989) except for LILEs and Pb. The gabbroic group (four samples) is characterized by positive Sr and Eu anomalies.

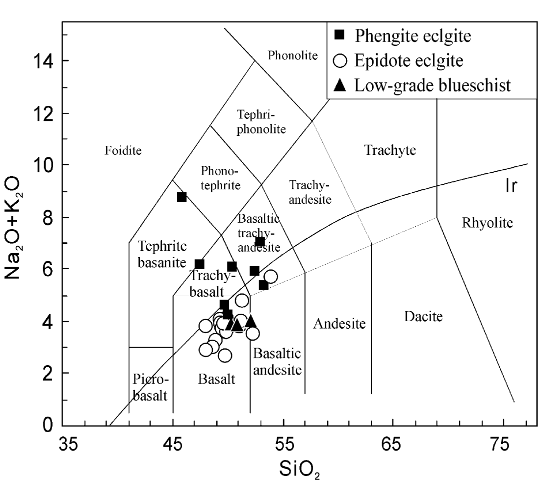


**Fig. 12.** Total alkali vs. $SiO_2$ (TAS) diagram for low-grade blueschists and two types of eclogites from the North Qilian suture zone. The boundary of alkaline and sub-alkaline (Ir) is after Irvine and Baragar (1971).

## 6. Temporal evolution of the high-pressure rocks

The North Qilian Mountain range has long been regarded as a "Caledonian" orogenic belt or plate suture zone in terms of the bio-stratigraphy (Wang and Liu, 1976; Xiao et al., 1978; Li et al., 1978). Geochronological studies of HPM rocks started in 1980s using K–Ar and $^{40}Ar$–$^{39}Ar$ methods on phengite and glaucophane for blueschists (Wu et al., 1993; Liou et al., 1989; Zhang et al., 1997; Liu et al., 2006). More recently, zircon U–Pb SHRIMP technique has been used to determine the metamorphic ages of eclogites (Song et al., 2004, 2006; Zhang et al., 2007). The low-grade blueschists, on the other hand, have not been precisely dated so far.

### *6.1. Ages for eclogite-facies metamorphism*

So far, five eclogite samples from the North Qilian HPM belt have been dated using zircon SHRIMP method by Song et al. (2004, 2006) and Zhang et al. (2007). Two samples from the Baijingsi cross-section (Fig. 6b) in the eastern part of the HPM belt yield 468 ± 13 Ma (Song et al., 2004) and 502 ± 11 Ma (Zhang et al., 2007); the latter age was shown to be a magmatic age of gabbroic protolith (Zhang et al., 2007). Three eclogite samples from the western part of the HPM belt give ages of 463 ± 6 Ma (Song et al., 2004), 477 ± 16 and 489 ± 7 Ma (Zhang et al., 2007), respectively.

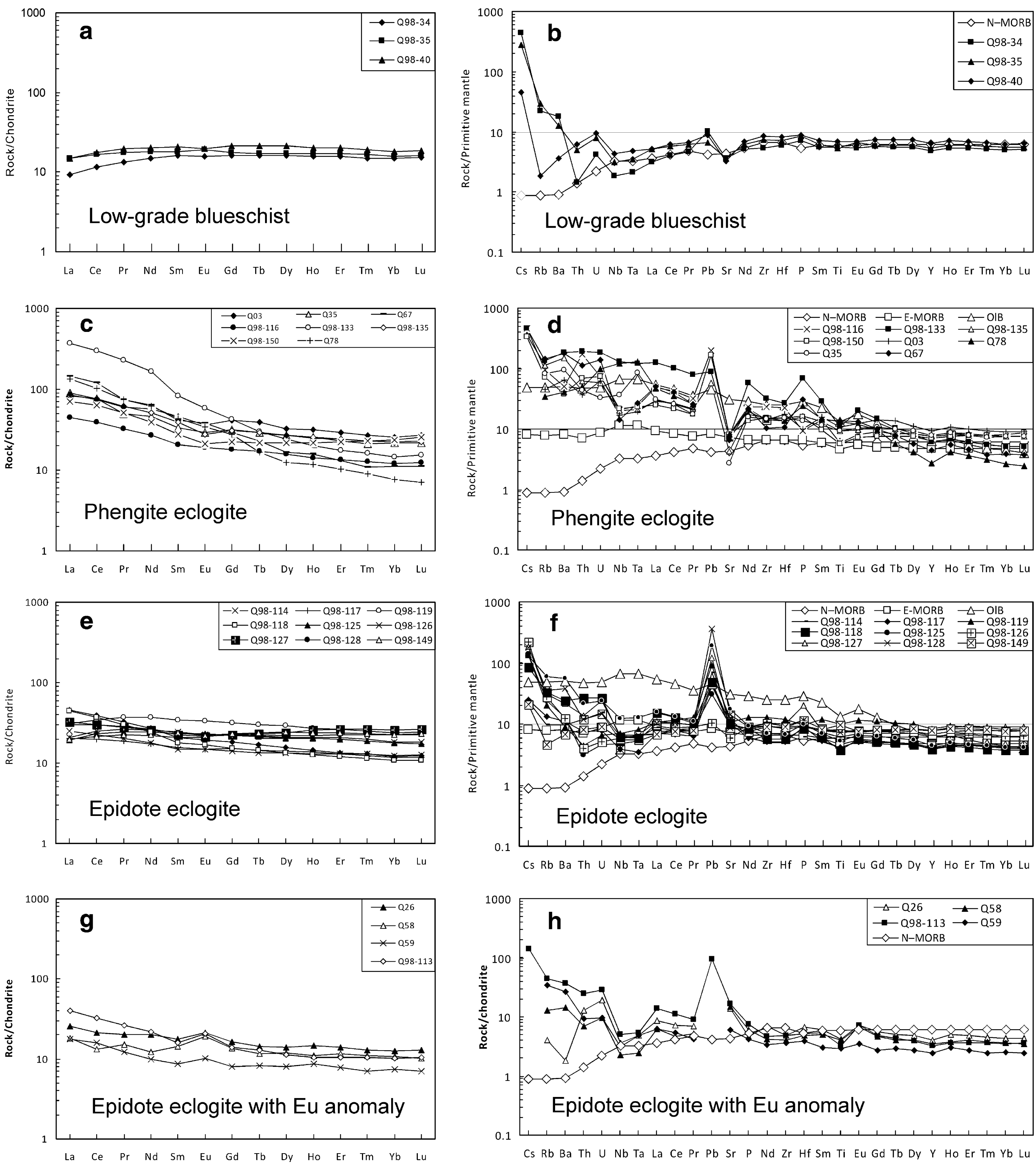


**Fig. 13.** Chondrite-normalized REE patterns and primitive mantle normalized spidergrams for mafic blueschist and two types of eclogite.

These ages are statistically similar, but the mean differences of ~20 m.y., if true, may reflect differences in the timing of eclogite-facies metamorphism in different eclogite blocks of the same HPM belt.

Plotting all zircon analyses of four eclogite samples yield metamorphic ages shown in Fig. 15. Four accumulate age peaks are 710–650, 544, 472 and 421 Ma. The old core ages of 710−650 Ma was interpreted as crustal contamination prior to subduction (Zhang et al., 2007), whereas the age of ~544 Ma for inherited magmatic zircon cores should represent the crust formation of the ancient "Qilian Ocean"; these ages are consistent with gabbroic zircon SHRIMP ages from the ophiolite complex (Shi et al., 2004; Tseng et al., 2007). The peak at ~472 Ma is accumulated from metamorphic ages (463–489 Ma) of the four eclogite samples and represent the timing of eclogite-facies metamorphism. The age peak at ~421 Ma (404–424 Ma) is distinctive, is consistent

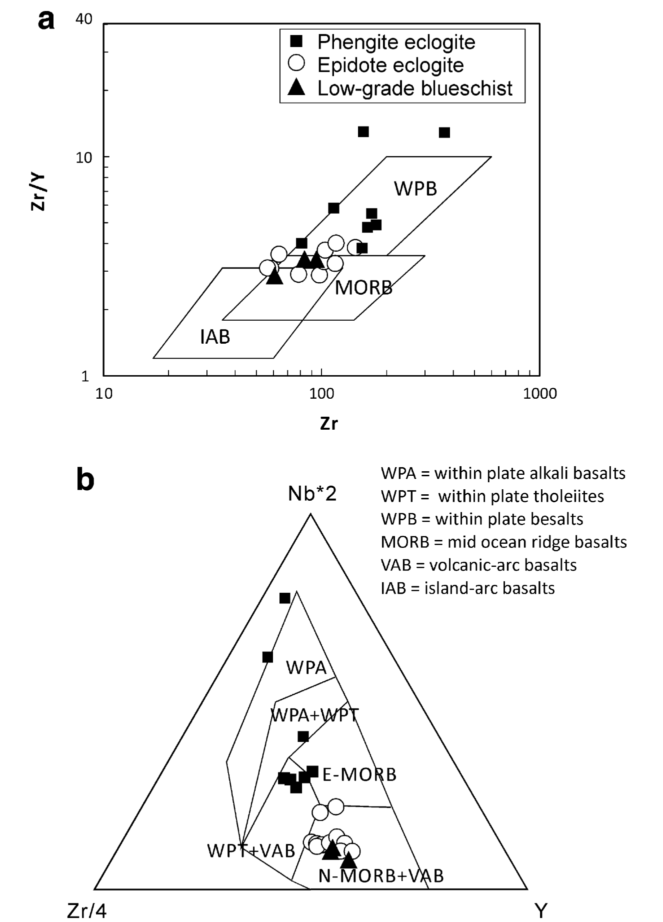


**Fig. 14.** Discrimination diagrams for low-grade blueschist and two types of eclogites.

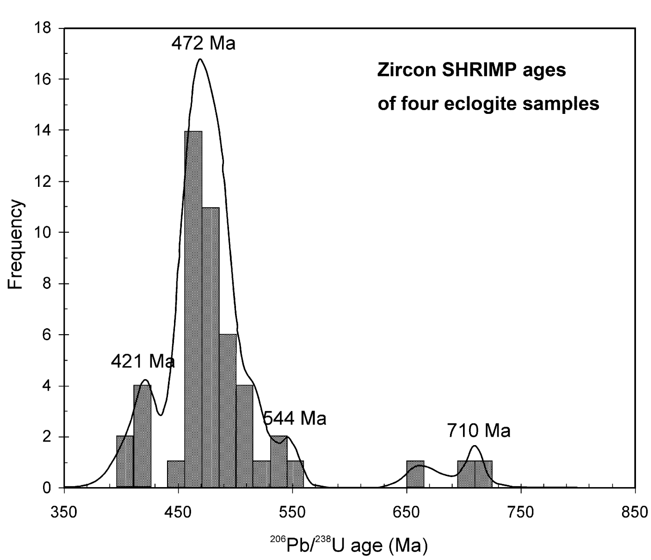


**Fig. 15.** Histogram of apparent $^{206}Pb/^{238}U$ age of all analyses (Song et al., 2004b, 2006; Zhang et al., 2007). Plots generated using ISOPLOT developed by Ludwig (2001).

with the Sm-Nd isochron age of the associated ophiolitic serpentinite (Smith and Yang, 2006), and is younger than the blueschist-facies metamorphism or cooling time of the HPM belt (see below). It represents a collision event overprinted on eclogites during the intense period of mountain building (molasse formation) in the North Qilian Mountains in Late Silurian–Early Devonian time. Moreover, this age is also consistent with the UHPM and exhumation ages of the North Qaidam *continental-type* subduction-zone inferred from dating of zircons from garnet-peridotites and coesite-bearing meta-pelites (~430–400 Ma, Song et al., 2005, 2006).

### *6.2. Ages for blueschist-facies metamorphism*

Ar–Ar dating of phengitic mica from high-grade blueschists yields plateau ages of 448 ± 11 Ma (Liou et al., 1989) and 446–454 Ma (Liu et al., 2006) and 450–489 Ma with retrograde overprint at 420–410 Ma for phengitic mica and glaucophane (Zhang et al., 1997).

Comparing these ages by re-examining the Ar–Ar age plateaus, the $^{40}Ar/^{39}Ar$ dating of phengitic mica yielded more reliable ages of 446–462 Ma than that of glaucophane (420–490 Ma, Zhang et al., 1997); therefore these phengitic mica ages should represent the major blueschist-facies metamorphism. Some $^{40}Ar/^{39}Ar$ ages of phengitic mica and glaucophane range from 420 to 400 Ma (Wu et al., 1993; Zhang et al., 1997) and most probably record the last exhumation event of the North Qilian HP belt corresponding to the orogenic uplift indicated by the deposition of the early Devonian molasses.

## 7. Discussion

### *7.1. Components of the subduction complex in North Qilian suture zone*

Protoliths of the North Qilian high-grade blueschist belt include four major components: (1) ophiolitic component with blocks of serpentinite, mafic eclogite and blueschist that represent the subducting oceanic slab, (2) blocks of pelagic and semi-pelagic sediments including meta-chert and meta-pelite, (3) marble, and (4) terrigenous trench greywacke and olistostrome. These rock assemblages are typical of accretionary complex or mélange in the context of seafloor subduction. Greywacke is volumetrically predominant, occupies more than half of the high-grade blueschist belt and accommodates other rock types as blocks. The geochemistry reveals that protoliths of eclogite and mafic blueschist have characteristics of present-day N-type and E-type mid-ocean ridge basalts (MROB). Mineral assemblages of these rocks indicate that they have been subducted to various depths and subjected to eclogite- to blueschist-facies metamorphism.

### *7.2. Determination of early Paleozoic oceanic "cold" subduction*

High-*P* and low-*T* metamorphic rocks together with ophoilitic complex at active continental margins represent ancient oceanic subduction-zones. Lawsonite and carpholite contain high-$H_2O$ that are only stable in a subduction-zone environment of low geothermal gradient. These two hydrous phases have been thought to be the diagnostic minerals for the "cold" oceanic subduction-zones, which requires that the ancient oceanic plates be large, old and have undergone a long time cooling since their birth at ocean ridges. If they descend fast, they would stay cold to great depth (Peacock and Wang, 1999).

Most cold oceanic subduction-zones with lawsonite and carpholite have been found in Tethyan belts with ages <80 Ma and no earlier than 500 Ma in Earth's orogenic belts (Agard et al., 2005). Only three HPM belts with similar ages of 450–490 Ma have been identified, i.e., Fe–Mg-carpholite-bearing blueschist and lawsonite-bearing eclogite in Motalafijella, Svalbard Caledonides (Hirajima et al., 1988; Agard et al., 2005), lawsonite-bearing eclogite in Port

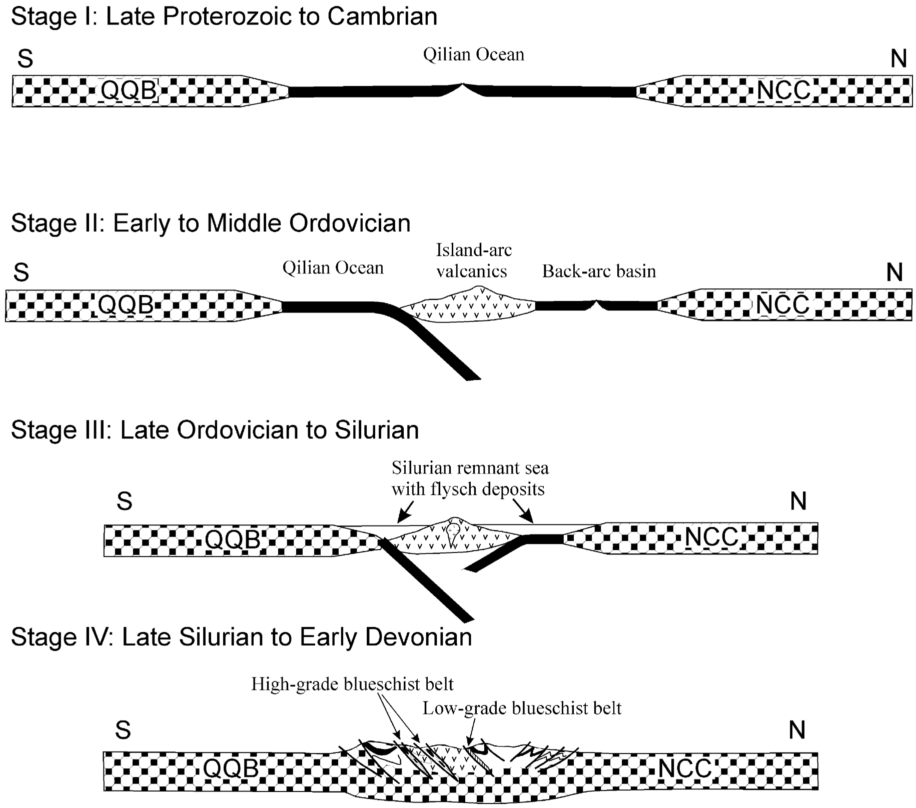


**Fig. 16.** Tectonic evolution of the North Qilian oceanic subduction-zone during early Paleozoic time. NCC – North China Craton, QQB – Qilian–Qaidam block.

Macquarie, New England fold belt, Australia (Och et al., 2003), and Mg-carpholite meta-pelite and lawsonite-bearing eclogite in the North Qilian suture zone (Song et al., 2007; Zhang et al., 2007).

Isotopic ages of HPM rocks (460–490 Ma) corroborate that the North Qilian is one of the three oldest occurrences of cold seafloor subduction thus far recognized on Earth. From lawsonite–pumpellyite–aragonite blueschist (250–350 °C, 0.60–1.2 GPa) to lawsonite eclogite and carpholite–chloritoid schist (460–530 °C, 2.20–2.60 GPa), we can deduce a progressive subduction path along a thermal gradient of 6–7 °C/km, which is similar to the other two Paleozoic subduction-zones in Motalafijella, Svalbard Caledonides (Hirajima et al., 1988; Agard et al., 2005) and the New England fold belt, Australia (Och et al., 2003). The deduced thermal gradient is as cold as some Cenozoic to present-day oceanic subduction-zones (e.g., Okay, 2002; Agard et al., 2001; Tsujimori et al., 2006). This could mean that the global mantle thermal gradient has had no significant change in the last 500 Ma of the Phanerozoic era. However, this interpretation can be erroneous because the geothermal gradient of an active subduction-zone is largely determined by the age, thickness, and subduction rate of a specific oceanic lithosphere, and cannot be used to infer global mantle thermal evolution. For example, the old and cold Pacific plate subduction beneath Northeast Japan takes a cold geotherm of ~5°/km, whereas the young and warm Philippine Plate subduction beneath Southwest Japan takes a warm geotherm of ~13°/km at present (Peacock and Wang, 1999).

### *7.3. Tectonic evolution of the North Qilian oceanic subduction-zone*

The tectonic evolution of the North Qilian seafloor subduction and orogenesis of the Qilian mountain belt has long been discussed (e.g. Wu et al., 1993; Xu et al., 1994; Feng and He, 1995; Yang et al., 2001, 2002; Yue et al., 2001; Xia et al., 2003; Song et al., 2006). Petrological and geochemical data, together with age dates, reveal that the suture zone rocks record a long tectonic history from ocean floor spreading, to oceanic lithosphere subduction, and to ultimate continental collision and mountain-building. Fig. 16 illustrates an inferred tectonic scenario in four stages. Stage I (Late Proterozoic to Cambrian): the Qilian Ocean may have existed in the Late Proterozoic to Cambrian (from >560 Ma to ~500 Ma), separating the North China Craton to the north and the Qilian–Qaidam Craton to the south. The Qilian–Qaidam Craton may be a fragment of the disintegrated Rodinia supercontinent with passive margins extending into oceanic lithosphere that floored the Qilian Ocean (Song et al., 2006). Stage II (Early to Middle Ordovician): oceanic lithosphere started to subduct northwards beneath western margin of the North China Craton along a cold geotherm of ~6–7 °C/km, and to undergo blueschist- and eclogite-facies metamorphism at the end of the Cambrian (ca. 500 Ma), accompanied by subduction-zone related mafic to felsic volcanism (e.g., island-arc, continental arc and perhaps back-arc as well). Stage III (Late Ordovician to Silurian): the Qilian Ocean closed at the Late Ordovician and the back-arc basin seafloor started to subduct southwards and form the low-grade blueschist belt. In the Silurian (~440–420 Ma), thick flysch sequence had deposited in a remnant sea. Stage IV (Late Silurian to Early Devonian): continental collision and orogenesis occurred at the Late Silurian and Devonian, which led to the mountain-building and uplifting, and as a result, the lower Devonian molasse deposited and HPM rock exhumation.

## Acknowledgements

We thank three anonymous reviewers and Bor-ming Jahn for their constructive review comments, which led to a better presentation of the final product. This study was supported by National

Natural Science Foundation of China (Grant Nos. 40773012, 40730314, and 40825007), the Foundation for the Author of National Excellent Doctoral Dissertation of China (200531), the Major State Basic Research Development Projects (2009CB825007) and by the science foundation of State Key Laboratory of Geological Processes and Mineral Resources, China University of Geosciences (GPMR200632).

## References

Agard, P., Labrousse, L., Elvevold, S., Lepvrier, C., 2005. Discovery of Palaeozoic Fe–Mg carpholite in Motalafjella, Svalbard Caledonides: a milestone for subduction-zone gradients. Geology 33, 761–764.

Agard, P., Vidal, O., Goffe, B., 2001. Interlayer and Si content of phengite in HP-LT carpholite-bearing metapelites. Journal of Metamorphic Geology 19, 479.

Batiza, R., Niu, Y., Zayac, W.C., 1990. Chemistry of seamounts near the East Pacific Rise: implications for the geometry of subaxial mantle flow. Geology 18, 1122–1125.

Batiza, R., Smith, T.L., Niu, Y., 1989. Geologic and petrologic evolution of seamounts near the EPR based on submersible and camera study. Marine Geophysical Research 11, 169–236.

Brown, E.H., 1977. The crossite content of Ca-amphibole as a guide to pressure of metamorphism. Journal of Petrology 18, 53–72.

Brown, M., 2007. Metamorphic conditions in orogenic belts: a record of secular change. International Geology Review 49, 193–234.

Bureau of Geology and Mineral Resources of Ningxia Province, 1990. Regional Geology of Ningxia Province. Geological Memoirs of Ministry of Geology and mineral Resources of People's Republic of China, Geological Publishing House, Beijing. 560p (in Chinese).

Cawthorn, R.G., Collerson, K.D., 1974. The recalculation of pyroxene end-member parameters and the estimation of ferrous and ferric iron content from electron microprobe analyses. American Mineralogist 59, 1203–1208.

Chen, N.S., Wang, Q.Y., Chen, Q., Li, X.Y., 2007. Components and metamorphism of the basements of the Qaidam and Oulongbuluke micro-continental blocks, and a tentative interpretation of paleocontinental evolution in NW-Central China. Earth Science Frontiers 14, 43–55 (in Chinese with English abstract).

Condie, K.C., 1997. Plate Tectonics and Crustal Evolution, fourth ed. Butterworth-Heinemann, Oxford. 282p.

Deer, W.A., Howie, R.A., Zussman, J., 1992. The Rock Forming Minerals, second ed. John Wiley & Sons Inc., New York. 696p.

Droop, G.T.R., 1987. A general equation for estimating $Fe^{3+}$ concentrations in ferromagnesian silicates and oxides from microprobe analyses, using stoichiometric criteria. Mineralogical Magazine 51, 431–435.

Ernst, W.G., 1972. Occurrence and mineralogical evolution of bluschist belts with time. American Journal of Science 272, 657–668.

Feng, Y.M., He, S.P., 1995. Research for geology and geochemistry of several ophiolites in the North Qilian Mountains, China. Geological Review 40, 252–264 (in Chinese with English abstract).

Geng, Y.S., Wang, X.S., Shen, Q.H., Wu, C.M., 2007. Chronology of the Precambrian metamorphic series in the Alxa area, Inner Mongolia. Geology in China 34, 251–261 (in Chinese with English abstract).

Hirajima, T., Banno, S., Hiroi, Y., Ohta, Y., 1988. Phase petrology of eclogites and related rocks from the Motalafjella high-pressure metamorphic complex in Spitsbergen and its significance. Lithos 22, 75–97.

Holland, T.J.B., Powell, R., 1998. An internally consistent thermodynamic data set for phases of petrological interest. Journal of Metamorphic Geology 16, 309–343.

Irvine, T.N., Baragar, W.R.A., 1971. A guide to the chemical classification of the common volcanic rocks. Canadian Journal of Earth Sciences 8, 523–548.

Kretz, R., 1983. Symbols for rock-forming minerals. American Mineralogist 68, 277–279.

Le Bas, M.J., LeMaitre, R.W., Streckeisen, R.W., Zanettin, B., 1986. A chemical classification of volcanic rocks based on the total alkali-silica diagram. Journal of Petrology 27, 745–750.

Li, C.Y., Liu, Y.W., Zhu, B.C., Feng, Y.M., Wu, H.Q., 1978. Structural evolutions of Qinling and Qilian. In: Editorial Office of Chinese Geological Bureau (Ed.), Scientific Papers on Geology for International Exchange. Geological Publishing House, Beijing, pp. 174–189 (in Chinese with English abstract).

Li, X.H., Su, L., Chung, S.L., Li, Z.X., Liu, Y., Song, B., Liu, D.Y., 2005. Formation of the Jinchuan ultramafic intrusion and the world's third largest Ni–Cu sulfide deposit: associated with the similar to 825 Ma south China mantle plume? Geochemistry Geophysics Geosystems 6, Q11004.

Liou, J., 1971. P-T stabilities of laumontite, wairakite, lawsonite, and related minerals in the system $CaAl_2Si_2O_8$–$SiO_2$–$H_2O$. Journal of Petrology 12, 370–411.

Liou, J.G., Maruyama, S., Cho, M., 1987. Very low-grade metamorphism of volcanic and volcaniclastic rocks – mineral assemblages and mineral facies. In: Frey, M. (Ed.), Very Low-grade Metamorphism. Blackie Published Co., pp. 59–113.

Liou, J.G., Maruyama, S., Wang, X., Graham, S.A., 1990. Precambrian blueschist terranes of the world. Tectonophysics 181, 97–111.

Liou, J.G., Wang, X., Coleman, R.G., 1989. Blueschists in major suture zones of China. Tectonics 8, 609–619.

Liu, Y.J., Neubauer, F., Genser, J., Takasu, A., Ge, X.-H., Handler, R., 2006. $^{40}Ar/^{39}Ar$ ages of blueschist facies pelitic schists from Qingshuigou in the Northern Qilian Mountains, western China. Island Arc 15, 187–198.

Ludwig, K.R., 2001. Users manual for Isoplot/Ex rev. 2.49. Berkeley Geochronology Centre Special Publication No. 1a, 56p.

Maruyama, S., Cho, M., Liou, J.G., 1986. Experimental investigations of blueschist-greenschist transition equilibra: pressure dependence of $Al_2O_3$ contents in sodic amphibole–A new geobarometer. Geological Society of America, Memoir 164, 1–16.

Maruyama, S., Liou, J.G., 1987. Clinopyroxene telescoped through the processes of blueschist facies metamorphism. Journal of Metamorphic Geology 5, 529–552.

Maruyama, S., Liou, J.G., 2005. From snowball to phanerozoic earth. International Geology Review 47, 775–791.

Maruyama, S., Liou, J.G., Terabayashi, M., 1996. Blueschists and eclogites of the world and their exhumation. International Geology Review 38, 485–594.

Mattinson, C.G., Wooden, J.L., Liou, J.G., Bird, D.K., Wu, C.L., 2006. Age and duration of eclogite-facies metamorphism, North Qaidam HP/UHP terrane, western China. American Journal of Science 306, 683–711.

Mattinson, C.G., Menold, C.A., Zang, J.X., Bird, D.K., 2007. High- and ultrahigh-pressure metamorphism in the North Qaidam and South Altyn Terranes, western China. International Geology Review 49, 969–995.

McGovern, P.J., Schubert, G., 1989. Thermal evolution of the earth: effects of volatile exchange between atmosphere and interior. Earth and Planetary Science Letters 96, 27–37.

Meschede, M., 1986. A method of discriminating between different types of mid-ocean ridge basalts and continental tholeiites with the Nb–Zr–Y diagram. Chemical Geology 56, 207–218.

Morimoto, N., 1988. Nomenclature of pyroxenes. Mineralogical Magazine 52, 535–550.

Niu, Y., Batiza, R., 1997. Trace element evidence from seamounts for recycled oceanic crust in the eastern equatorial Pacific mantle. Earth and Planetary Science Letters 148, 471–484.

Niu, Y., 2004. Bulk-rock major and trace element compositions of abyssal peridotites: surprises and implications for mantle melting, melt extraction and post-melting processes beneath ocean ridges. Journal of Petrology 45, 2423–2458.

Och, D.J., Leitch, E.C., Caprarelli, G., Watanabe, T., 2003. Blueschist and eclogite in tectonic melange, Port Macquarie, New South Wales. Australian Mineralogy Magazine 67, 609–624.

Okay, A.I., 2002. Jadeite–chloritoid–glaucophane–lawsonite blueschists in northwest Turkey: unusually high P/T ratios in continental crust. Journal of Metamorphic Geology 20, 757–768.

Peacock, S.M., Wang, K., 1999. Seismic consequences of warm versus cool subduction metamorphism: examples from southwest and northeast Japan. Science 286, 937–939.

Pearce, J.A., Norry, M.J., 1979. Petrogenetic implications of Ti, Zr, Y and Nb variations in volcanic rocks. Contributions to Mineralogy and Petrology 69, 33–47.

Powell, R., Holland, T.J.B., Worley, B., 1998. Calculating phase diagrams involving solid solutions via non-linear equations, with examples using Thermocalc. Journal of Metamorphic Geology 16, 577–588.

Qian, Q., Zhang, Q., Sun, X.M., 2001. Tectonic setting and mantle source characteristics of Jiugequan basalts, North Qilian: constraints from trace elements and Nd-isotopes. Acta Petrologica Sinica 17, 385–394 (in Chinese with English abstract).

Ravna, E.J.K., Terry, M.P., 2004. Geothermobarometry of UHP and HP eclogites and schists – an evaluation of equilibria among garnet–clinopyroxene–kyanite–phengite–coesite/quartz. Journal of Metamorphic Geology 22, 579–592.

Robinson, P., Spear, F.S., Schumacher, J.C., Laird, J., Klein, C., Evans, B.W., Doolan, B.L., 1982. Phase relations of metamorphic amphiboles: natural occurrence and theory. In: Veblen, D.R., Ribbe, P.H. (Eds.), Mineralogical Society of America, Reviews in Mineralogy 9B, 1–227.

Rudnick, R.L., Gao, S., Ling, W.L., Liu, Y.S., McDonough, W.F., 2004. Petrology and geochemistry of spinel peridotite xenoliths from Hannuoba and Qixia, North China craton. Lithos 77, 609–637.

Schiffman, P., Liou, J.G., 1980. Synthesis and stability relations of Mg–Al pumpellyite, $Ca_4Al_5MgSi_6O_{21}(OH)_7$. Journal of Petrology 21, 441–474.

Shi, R.D., Yang, J.S., Wu, C.L., Wooden, J., 2004. First SHRIMP dating for the formation of the late Sinian Yushigou Ophiolite, North Qilian Mountains. Acta Geologica Sinica 78, 649–657.

Smith, A.D., Yang, H.-Y., 2006. The neodymium isotopic and geochemical composition of serpentinites from ophiolitic assemblages in the Qilian fold belt, northwest China. Journal of Asian Earth Sciences 28, 119–132.

Song, S.G., 1996. Metamorphic geology of blueschists, eclogites and ophiolites in the North Qilian Mountains. In: Proceedings of the 30th IGC Field Trip Guide T392. Geological Publishing House, Beijing. 40p.

Song, S.G., 1997. Tectonic evolution of subductive complex belts in the North Qilian Mountains. Advances in Earth Sciences 12, 351–365 (in Chinese with English abstract).

Song, S.G., Yang, J.S., Liou, J.G., Wu, C.L., Shi, R.D., Xu, Z.Q., 2003a. Petrology, geochemistry and isotopic ages of eclogites in the Dulan UHPM terrane, the North Qaidam, NW China. Lithos 70, 195–211.

Song, S.G., Yang, J.S., Xu, Z.Q., Liou, J.G., Shi, R.D., 2003b. Metamorphic evolution of the coesite-bearing ultrahigh-pressure terrane in the North Qaidam, northern Tibet, NW China. Journal of Metamorphic Geology 21, 631–644.

Song, S.G., Zhang, L.F., Niu, Y.L., 2004a. Ultra-deep origin of garnet peridotite from the North Qaidam ultrahigh-pressure belt, Northern Tibetan Plateau, NW China. American Mineralogist 89, 1330–1336.

Song, S.G., Zhang, L.F., Niu, Y.L., Song, B., Zhang, G.B., Wang, Q.J., 2004b. Zircon U–Pb SHRIMP ages of eclogites from the North Qilian Mountains, NW China and their tectonic implication. Chinese Science Bulletin 49, 848–852.

Song, S.G., Zhang, L.F., Niu, Y.L., Su, L., Jian, P., Liu, D.Y., 2005. Geochronology of diamond-bearing zircons from garnet-peridotite in the North Qaidam UHPM belt, North Tibetan Plateau: a record of complex histories associated with continental collision. Earth Planetary Science Letters 234, 99–118.

Song, S.G., Zhang, L.F., Niu, Y.L., Su, L., Song, B., Liu, D.Y., 2006. Evolution from oceanic subduction to continental collision: a case study of the Northern Tibetan Plateau inferred from geochemical and geochronological data. Journal of Petrology 47, 435–455.

Song, S.G., Zhang, L.F., Niu, Y.L., Wei, C.J., Liou, J.G., Shu, G.M., 2007. Eclogite and carpholite-bearing meta-pelite in the North Qilian suture zone, NW China: implications for Paleozoic cold oceanic subduction and water transport into mantle. Journal of Metamorphic Geology 25, 547–563.

Sun, S.-S., McDonough, W.F., 1989. Chemical and isotopic systematics of oceanic basalt: implications for mantle composition and processes. In: Saunders, A.D., Norry, M.J. (Eds.), Magmatism in the Ocean Basins, vol. 42. Geological Society of London, Special Publication, pp. 313–345.

Tseng, C.Y., Yang, H.J., Yang, H.Y., Liu, D.Y., Tsai, C.L., Wu, H.Q., Zuo, G.C., 2007. The Dongcaohe ophiolite from the North Qilian Mountains: a fossil oceanic crust of the Paleo-Qilian ocean. Chinese Science Bulletin 52, 2390–2401.

Tsujimori, T., Sisson, V.B., Liou, J.G., Harlow, G.E., Sorensen, S.S., 2006. Very-low-temperature record of the subduction process: a review of worldwide lawsonite eclogites. Lithos 92, 609–624.

Tung, K.A., Yang, H.Y., Liu, D.Y., Zhang, J.X., Tseng, C.Y., Wan, Y.S., 2007a. SHRIMP U–Pb geochronology of the detrital zircons from the Longshoushan group and its tectonic significance. Chinese Science Bulletin 52, 1414–1425.

Tung, K.A., Yang, H.J., Yang, H.Y., Liu, D.Y., Zhang, J.X., Wan, Y.S., Tseng, C.Y., 2007b. SHRIMP U–Pb geochronology of the zircons from the Precambrian basement of the Qilian Block and its geological significances. Chinese Science Bulletin 52, 2687–2701.

Wan, Y.S., Xu, Z.Q., Yang, J.S., 2001. Ages and compositions of the Precambrian high-grade basement of the Qilian terrance and its adjacent areas. Acta Geologica Sinica 75, 375–384.

Wang, Q., Liu, X.Y., 1976. The ancient oceanic crust and its tectonic implications, North Qilian Mountains, China. Scienta Geologica Sinica (1), 42–55 (in Chinese with English abstract).

Wei, C.J., Song, S.G., 2008. Chloritoid–glaucophane schist in the north Qilian orogen, NW China: phase equilibria and P-T path from garnet zonation. Journal of Metamorphic Geology 26, 301–316.

Wu, C.L., Yang, J.S., Yang, H.Y., Wooden, J.L., Shi, R.D., Chen, S.Y., Zheng, Q.G., 2004. Dating of two types of granite from north Qilian, China. Acta Petrologica Sinica, 425–432 (in Chinese with English abstract).

Wu, H.Q., Feng, Y.M., Huo, Y.G., Zuo, G.C., 1990. Discovery of lawsonite glaucophane schist and the signification in Sunan, Gansu, China. Geological Review 36, 277–280.

Wu, H.Q., Feng, Y.M., Song, S.G., 1993. Metamorphism and deformation of blueschist belts and their tectonic implications, North Qilian Mountains, China. Journal of Metamorphic Geology 11, 523–536.

Xia, L.Q., Xia, Z.C., Xu, X.Y., 2003. Magmageneisis in the Ordovician in back basins of the northern Qilian Mountains, China. Geological Society of America Bulletin 115, 1510–1522.

Xiao, X.C., Chen, G., Zhu, Z.Z., 1978. A preliminary study on the tectonics of ancient ophiolites in the Qilian Mountain, Northwest China. Acta Geologica Sinica 54, 281–295 (in Chinese with English abstract).

Xiu, Q.Y., Yu, H.F., Li, Q., Zuo, G.C., Li, J.W., Cao, C.J., 2004. Discussion on the petrogenic time of Longshoushan Group, Gansu Province. Acta Geologica Sinica 78, 366–373.

Xu, W.C., Zhang, H.F., Liu, X.M., 2007. U–Pb zircon dating constraints on formation time of Qilian high-grade metamorphic rock and its tectonic implications. Chinese Science Bulletin 52, 531–538.

Xu, Z.Q., Xu, H.F., Zhang, J.X., Li, H.B., Zhu, Z.Z., Qu, J.C., Yang, K.C., 1994. The Zhoulangnanshan Caledonian subductive complex in the Northern Qilian Mountains and its dynamics. Acta Geologica Sinica 68, 1–15.

Yue, Y.J., Liou, J.G., Graham, S.A., 2001. Tectonic correlation of Beishan and Inner Mongolia orogens and its implications for the palinspastic reconstruction of north China. In: Hendrix, M.S., Davis, G.A. (Eds.), Paleozoic and Mesozoic tectonic evolution of central Asia: from continental assembly to intracontinental deformation. Geological Society of America, Memoir, 194, 101–116.

Yang, J.S., Xu, Z.Q., Song, S.G., et al., 2001a. Discovery of coesite in the North Qaidam early Palaeozoic ultrahigh pressure (UHP) metamorphic belt, NW China. Comptes Rendus De L Academie Des Sciences Serie II Fascicule A-Sciences De La Terre et des Planetes 333, 719–724.

Yang, J.S., Xu, Z.Q., Zhang, J.X., Chu, J.Y., Zhang, R.Y., Liou, J.G., 2001b. Tectonic significance of Caledonian high-pressure rocks in the Qilian - Qaidam - Altun Mountains, NW China. In: Hendrix, M.S., Davis, G.A. (Eds.), Paleozoic and Mesozoic tectonic evolution of central Asia: from continental assembly to intracontinental deformation. Geological Society of America, Memoir 194, 151–170.

Yang, J.S., Xu, Z.Q., Zhang, J.X., Song, S.G., Wu, C.L., Shi, R.D., Li, H.B., Brunel, M., 2002. Early Palaeozoic North Qaidam UHP metamorphic belt on the north-eastern Tibetan plateau and a paired subduction model. Terra Nova 14, 397–404.

Zhang, J.X., Xu, Z.Q., Chen, W., Xu, H.F., 1997a. A tentative discussion on the ages of the subduction – accretionary complex/volcanic arcs in the middle sector of North Qilian Mountain. Acta Petrologica et Mineralogica 16, 112–119 (in Chinese with English abstract).

Zhang, J.X., Zhang, Z.M., Xu, Z.Q., Yang, J.S., Cui, J.W., 2001. Petrology and geochronology of eclogites from the western segment of the Altyn Tagh, Northwestern China. Lithos 56, 187–206.

Zhang, J.X., Meng, F.C., Wan, Y.S., Yang, J.S., Tung, K.A., 2003. Early Paleozoic tectono-thermal event of the Jingshuikou Group on the South margin of Qaidam: zircon U–Pb SHRIMP age evidence. Geological Bulletin of China 22, 397–404 (in Chinese with English abstract).

Zhang, J.X., Yang, J.S., Meng, F.C., Wan, Y.S., Li, H.M., Wu, C.L., 2006. U–Pb isotopic studies of eclogites and their host gneisses in the Xitieshan area of the North Qaidam Mountains, western China: new evidence for an early Paleozoic HP-UHP metamorphic belt. Journal of Asian Earth Sciences 28, 143–150.

Zhang, J.X., Meng, F.C., Wan, Y.S., 2007. A cold early Palaeozoic subduction zone in the North Qilian Mountains, NW China: petrological and U–Pb geochronological constraints. Journal of Metamorphic Geology 25, 285–304.

Zhang, Q., Sun, X., Zhou, D., Qian, Q., Chen, Y, Wang, Y., Jia, X., Han, S., 1997b. The characteristics of North Qilian ophiolites, forming settings and their tectonic significance. Advance in Earth Sciences 12, 366–393 (in Chinese with English abstract).